

Change-Point Testing for Risk Measures in Time Series*

Lin Fan[†]

Junting Duan[‡]

Peter Glynn[§]

Markus Pelger[¶]

This draft: September 25, 2025

First draft: September 10, 2018

Abstract

We propose novel methods for change-point testing for nonparametric estimators of expected shortfall and related risk measures in weakly dependent time series. We can detect general multiple structural changes in the tails of marginal distributions of time series under general assumptions. Self-normalization allows us to avoid the issues of standard error estimation. The theoretical foundations for our methods are functional central limit theorems, which we develop under weak assumptions. An empirical study of S&P 500 and US Treasury bond returns illustrates the practical use of our methods in detecting and quantifying instability in the tails of financial time series.

Keywords: Time Series, Risk Measure, Change-Point Test, Confidence Interval, Self-Normalization, Sectioning, Expected Shortfall, Unsupervised Change Point Detection

JEL classification: C14, C58, G32

*We thank seminar and conference participants at Stanford and the NBER-NSF Time-Series Conference for helpful comments.

[†]Northwestern University, Kellogg School of Management, Email: lin.fan@kellogg.northwestern.edu.

[‡]Stanford University, Department of Management Science & Engineering, Email: duanjt@stanford.edu.

[§]Stanford University, Department of Management Science & Engineering, Email: glynn@stanford.edu.

[¶]Stanford University, Department of Management Science & Engineering, Email: mpelger@stanford.edu.

1 Introduction

The quantification of risk is a central topic of study in finance. The need to guard against unforeseeable events with adverse and potentially catastrophic consequences has led to an extensive and burgeoning literature on risk measures. The two most popular financial risk measures, the value-at-risk (VaR) and the expected shortfall (ES), are extensively used for risk and portfolio management as well as regulation in the finance industry (McNeil et al., 2015). Parallel to the developments in risk estimation, there has been longstanding interest in detecting changes in financial time series, especially changes in the tail structure, which is essential for effective risk and portfolio management. Indeed, empirical findings strongly suggest that financial time series frequently exhibit changes in their underlying statistical structure due to changes in economic conditions, e.g. monetary policies, or critical social events. Although there is an established literature on structural change detection for parametric time series models, including monitoring of proxies for risk such as tail index, there is little work concerning monitoring of general tail structure, or of risk measures in particular. To underscore this point, the existing literature on risk measure estimation assumes stationarity of time series observations over a time period of interest, with the stationarity of the risk measure being key for the estimation to make sense. However, it is a challenge to verify this assumption.

We provide tools to detect general and potentially multiple changes in the tail structure of time series, and in particular, tools for monitoring for changes in risk measures such as ES and related measures such as conditional tail moments (CTM) (Mehni et al., 2014) over time periods of interest. Specifically, we develop retrospective change-point tests to detect changes in ES and related risk measures. Additionally, we offer new ways of constructing confidence intervals for these risk measures. Our methods are applicable to a wide variety of time series models as they depend on functional central limit theorems for the risk measures, which we develop under weak assumptions. As described below, our methods complement and extend the existing literature in several ways.

As mentioned previously, the literature lacks tools to monitor general tail structure or risk measures such as ES or CTM over time. This deficiency appears to be two-fold. (1) Although there are studies on VaR change-point testing, for example, Qu (2008), often one is interested in characterizations of tail structure that are more informative than simple location measures. Indeed, the introduction of ES as an alternative risk measure to VaR was, to a great extent, driven by the need to quantify tail structure, particularly, the expected magnitude of losses conditional on losses being in the tail. Aligned with this goal, a popular measure of tail structure is the tail index, which describes tail thickness and governs distributional moments. In tail index estimation, an extreme value theory approach is typically taken with the assumption of so-called regularly-varying Pareto-type tails. However, tail index estimation is very sensitive to the choice of which fraction of sample observations is classified to be “in the tail”.¹ Moreover, the typical regularly-varying

¹The Hill estimator (Hill, 1975) is widely used and requires the user to choose the fraction of sample observations deemed to be “in the tail” to use for estimation. However, generally, there appears to be no best way to select this fraction. In the specific setting of change-point testing for tail index, recommendations for this fraction in the literature range from the top 20th percentile to the top 5th percentile of observations (Kim and Lee, 2009, 2011; Hoga, 2017). Such choice heavily influences the quality of tail index estimation and change detection and must be made on a case-by-case basis (Rocco, 2014). It is a delicate matter as choosing too small of a fraction results in high

Pareto-type tail assumptions may not even be valid in some situations. And even if they are valid, the tail index is invariant to changes of the location and scale types, and thus these types of structural changes in the tail would remain undetected using tail index-based change-point tests. (2) As mentioned before, all previous studies on risk measure estimation implicitly assume the risk measure is constant over some time period of interest—otherwise, risk measure estimation and confidence interval construction could behave erratically. For instance, if there is a sudden change in VaR (at some level) in the middle of a time series, naively estimating VaR using the entire time series could result in a wrong estimate of VaR or ES. Hence, given the importance of ES and related risk measures, a simple test for ES change over a time period of interest is a useful first step prior to follow-up statistical analysis.

To simultaneously address both deficiencies, we propose retrospective change-point testing for ES and related risk measures such as CTM. We introduce, in particular, a consistent test for a potential ES change at an unknown time based on a variant of the widely used cumulative sum (CUSUM) process.² We subsequently generalize this test to the case of multiple potential ES change points, leveraging recent work by Zhang and Lavitas (2018), and unlike existing change-point testing methodologies in the literature, our test does not require the number of potential change points to be specified in advance. Our use of a risk measure such as ES is attractive in many ways. First, the fraction of observations used in ES estimation, for example, the upper 5th percentile of observations, directly has meaning, and is often comparable to the fraction of observations used in tail index estimation, as discussed previously. Second, the use of ES does not require parametric-type tail assumptions, which is not the case with use of the tail index. Third, ES can detect much more general structural changes in the tail such as location or scale changes, while such changes go undetected when using tail index. Moreover, our change-point tests can be used to check in a statistically principled way whether or not ES and related risk measures are constant over a time period of interest, and provide additional validity when applying existing estimation methods for these risk measures.

A key detail that has been largely ignored in previous studies is standard error estimation. Here, the issue is two-fold. (1) In the construction of confidence intervals for risk measures, consistent estimation of standard errors is nontrivial due to standard errors involving the entire time series correlation structure at all integer lags, and thus being infinite-dimensional in nature. A few studies in which standard error estimation has been addressed (or bypassed) are Chen and Tang (2005); Chen (2008); Wang and Zhao (2016); Xu (2016). However, confidence interval construction in these studies all require user-specified tuning parameters such as the bandwidth in periodogram kernel smoothing or window width in the blockwise bootstrap and empirical likelihood methods. Although the choice of these tuning parameters significantly influences the quality of the resulting confidence intervals, it is not always clear how to best to select them. (2) Choosing the tuning parameters is not only difficult, but data-driven approaches may result in non-monotonic test power, as pointed out in numerous studies (Vogelsang, 1999; Crainiceanu and Vogelsang, 2007; Deng and Perron,

estimation variance and choosing too large of a fraction often results in high bias due to misspecification of where the tail begins.

²The cumulative sum (CUSUM) process was first introduced by Page (1954) and is discussed in detail in Csorgo and Horvath (1997).

2008; Shao and Zhang, 2010).³

We offer the following solutions to the above issues. (1) To address the issue of often problematic selection of tuning parameters for confidence interval construction with time series data, we make use of ratio statistics to cancel out unknown standard errors and form pivotal quantities, thereby avoiding the often difficult estimation of such nuisance parameters. We examine confidence interval construction using a technique originally referred to in the simulation literature as sectioning (Asmussen and Glynn, 2007), which involves splitting the data into equal-size non-overlapping sections, separately evaluating the estimator of interest using the data in each section, and relying on a normal approximation to form an asymptotically pivotal t-statistic. We also examine its generalization, referred to in the simulation literature as standardized time series (Schruben, 1983; Glynn and Iglehart, 1990) and in the time series literature as self-normalization (Lobato, 2001; Shao, 2010), which uses functionals different from the t-statistic to create asymptotically pivotal quantities. (2) In the context of change-point testing using ES and related risk measures, to avoid potentially troublesome standard error estimation, we follow Shao and Zhang (2010) and Zhang and Lavitas (2018) and apply the method of self-normalization for change-point testing by dividing CUSUM-type processes by corresponding processes designed to cancel out the unknown standard error. The processes we divide by take into account potential change point(s) and thus avoids the problem of non-monotonic power which often plagues change-point tests that rely on consistent standard error estimation, as discussed previously.

The outline of our paper is as follows. We describe the setting and assumptions in Section 2.1. In Section 2.2, we develop the asymptotic theory for VaR and ES, specifically, functional central limit theorems, which provide the theoretical basis for the proposed confidence interval construction and change-point testing methodologies. In introducing our statistical methods, we first discuss the simpler task of confidence interval construction for risk measures in Section 3.1. Then, with several fundamental ideas in place, we take up testing for a single potential change point in VaR and ES in Section 3.2. We extend the change-point testing methodology to an unknown, possibly multiple, number of change points in Section 3.3. In Section 4, we demonstrate the good finite-sample performance of our proposed methods through simulations. We conclude with an empirical study in Section 5 of returns data for the S&P 500 index and US Treasury bond returns. The proofs of our theoretical results as well as additional simulation and empirical results can be found in the Appendix.

2 Asymptotic Theory

2.1 Model Setup

Suppose the random variable X and the stationary sequence of random variables X_1, \dots, X_n have the marginal distribution function F . For some level $p \in (0, 1)$, we want to estimate the risk

³For general change-point tests with time series observations, consistent estimation of standard errors is typically done using periodogram kernel smoothing, and the performance of such tests is heavily influenced by the choice of kernel bandwidth.

measures VaR (value-at-risk) and ES (expected shortfall) defined by:⁴

$$VaR = \inf\{x \in \mathbb{R} : F(x) \geq p\}$$

$$ES = \mathbb{E}[X \mid X \geq VaR].$$

Let $\widehat{F}_n(\cdot) = n^{-1} \sum_{i=1}^n \mathbb{I}(X_i \leq \cdot)$ be the sample distribution function. We consider the following plug-in sample-based nonparametric estimators:

$$\widehat{VaR}_n = \inf\{x \in \mathbb{R} : \widehat{F}_n(x) \geq p\} \quad (1)$$

$$\widehat{ES}_n = \frac{1}{1-p} \frac{1}{n} \sum_{i=1}^n X_i \mathbb{I}\left(X_i \geq \widehat{VaR}_n\right). \quad (2)$$

For the change-point testing, we estimate these risk measures on subsets of the data. Hence, for $m > l$, we will also consider the following nonparametric estimators based on samples X_l, \dots, X_m , with $\widehat{F}_{l:m}(\cdot) = (m-l+1)^{-1} \sum_{i=l}^m \mathbb{I}(X_i \leq \cdot)$:

$$\widehat{VaR}_{l:m} = \inf\{x \in \mathbb{R} : \widehat{F}_{l:m}(x) \geq p\} \quad (3)$$

$$\widehat{ES}_{l:m} = \frac{1}{1-p} \frac{1}{m-l+1} \sum_{i=l}^m X_i \mathbb{I}\left(X_i \geq \widehat{VaR}_{l:m}\right). \quad (4)$$

We derive the asymptotic theory under general assumptions for the stochastic process. Let \mathcal{F}_l^m denote the σ -algebra generated by X_l, \dots, X_m , and let \mathcal{F}_l^∞ denote the σ -algebra generated by X_l, X_{l+1}, \dots . The α -mixing coefficient, as introduced by Rosenblatt (1956), is defined as

$$\alpha(k) = \sup_{A \in \mathcal{F}_1^j, B \in \mathcal{F}_{j+k}^\infty, j \geq 1} |\mathbb{P}(A)\mathbb{P}(B) - \mathbb{P}(A, B)|,$$

and a sequence is said to be α -mixing if $\lim_{k \rightarrow \infty} \alpha(k) = 0$. The dependence described by α -mixing is the least restrictive as it is implied by the other types of mixing; see Doukhan (1994) for a comprehensive discussion. In what follows, $D[0, 1]$ denotes the space of real-valued functions on $[0, 1]$ that are right-continuous and have left limits, and convergence in distribution on this space is defined with respect to the Skorohod topology (Billingsley, 1999). Also, for some index set \mathcal{I} , $\ell^\infty(\mathcal{I})$ denotes the space of real-valued bounded functions on \mathcal{I} , and convergence in distribution on this space is defined with respect to the uniform topology. We denote the integer part of a real number x by $[x]$ and the positive part by $[x]_+$. A standard Brownian motion on the real line is denoted by W . Our theoretical results are developed using the following assumption.

Assumption 1. *For some constants $\gamma > 0$ and $a > \max(3, (2 + \gamma)/\gamma)$:*

(i) X_1, X_2, \dots is α -mixing with $\alpha(k) = O(k^{-a})$

(ii) $\mathbb{E}[|X|^{2+\gamma}] < \infty$

(iii) X has a positive and differentiable density f in a neighborhood of VaR , and for each $k \geq 2$, (X_1, X_k) has joint density in a neighborhood of (VaR, VaR) .

⁴It is reasonable to define VaR and ES as upper tail characteristics when considering a loss process.

Assumption 1 condition (i) is a form of asymptotic independence, which ensures that the time series is not too serially dependent so that non-degenerate limit distributions are possible. A very wide range of commonly used financial time series models such as GARCH models and diffusion models satisfy this condition. Condition (ii) indicates a trade-off between the strength of the moment condition of the underlying marginal distribution and the rates of α -mixing, with weaker α -mixing conditions requiring stronger moment conditions and vice versa. Condition (iii) is a standard assumption in VaR and ES estimation, and rules out pathological situations in which there are many ties among the observations near VaR .

We point out, in particular, that while our results are illustrated for the most widely used risk measures, VaR and ES, they can be adapted to many other important functionals of the underlying marginal distribution. One straightforward adaptation (by assuming stronger α -mixing and moment conditions) is to CTM: $\mathbb{E}[X^\beta | X > VaR]$ for some level $p \in (0, 1)$ and some $\beta > 0$ (Methni et al., 2014). Our results also easily extend to multivariate time series, but for simplicity of illustration, we focus on univariate time series.

2.2 Functional Central Limit Theorems

We develop functional central limit theorems jointly for VaR and ES under weak assumptions. These functional central limit theorems allow the construction of general change point statistics.

Theorem 1. *Under Assumption 1, the process*

$$\left\{ \sqrt{nt} \begin{bmatrix} \widehat{VaR}_{[nt]} - VaR \\ \widehat{ES}_{[nt]} - ES \end{bmatrix} : t \in [0, 1] \right\} \quad (5)$$

converges in distribution in $D[0, 1] \times D[0, 1]$ to $\Sigma^{1/2}(W_1, W_2)$, where W_1 and W_2 are independent standard Brownian motions, and $\Sigma \in \mathbb{R}^{2 \times 2}$ is symmetric positive-semidefinite with components

$$\Sigma_{11} = \frac{1}{f^2(VaR)} \left(\mathbb{E}[g^2(X_1)] + 2 \sum_{i=2}^{\infty} \mathbb{E}[g(X_1)g(X_i)] \right) \quad (6)$$

$$\Sigma_{12} = \frac{1}{f(VaR)(1-p)} \left(\mathbb{E}[g(X_1)h(X_1)] + \sum_{i=2}^{\infty} (\mathbb{E}[g(X_1)h(X_i)] + \mathbb{E}[h(X_1)g(X_i)]) \right) \quad (7)$$

$$\Sigma_{22} = \frac{1}{(1-p)^2} \left(\mathbb{E}[h^2(X_1)] + 2 \sum_{i=2}^{\infty} \mathbb{E}[h(X_1)h(X_i)] \right), \quad (8)$$

where $g(X) = \mathbb{I}(X \leq VaR) - p$ and $h(X) = [X - VaR]_+ - \mathbb{E}[[X - VaR]_+]$.

Our Assumption 1 conditions (i)-(ii) are weaker than those of existing central limit theorems in the literature (c.f. Chen and Tang (2005); Chen (2008)), which require α -mixing coefficients to decay exponentially fast, as well as additional regularity of the marginal and pairwise joint densities of the observations.

In deriving the ES functional central limit theorem, we used the following Bahadur representation for \widehat{ES}_n .

Proposition 1. Suppose Assumption 1 holds for some $\gamma > 0$ and $a > (2 + \gamma)/\gamma$. Then, for any $\gamma' > 0$ satisfying $-1/2 + 1/(2a) + \gamma' < 0$,

$$\widehat{ES}_n - \left(VaR + \frac{1}{1-p} \frac{1}{n} \sum_{i=1}^n [X_i - VaR]_+ \right) = o_{a.s.}(n^{-1+1/(2a)+\gamma'} \log n).$$

Sun and Hong (2010) developed such a Bahadur representation in the setting of independent, identically-distributed data, but to the best of our knowledge, no such representation exists in the stationary, α -mixing setting. Such a Bahadur representation is generally useful for developing limit theorems in many different contexts.

We also have the following extension of the functional central limit theorems for VaR and ES in Theorem 1, where now there are two “time” indices instead of just one. The standard functional central limit theorems are useful for detecting a single change point in a time series, but the following extension will allow us to detect an unknown, possibly multiple, number of change points, as we will discuss later. We point out that this result does not follow automatically from Theorem 1 and an application of the continuous mapping theorem, because the estimators in (3)-(4) are not additive, for instance, for $m > l$, $\widehat{ES}_{l:m} \neq \widehat{ES}_{1:m} - \widehat{ES}_{1:l-1}$.

Theorem 2. Fix any $\delta > 0$ and consider the index set $\Delta = \{(s, t) \in [0, 1]^2 : t - s \geq \delta\}$. Under Assumption 1, with the modification that (X_1, X_k) has a joint density for all $k \geq 2$, the process

$$\left\{ \sqrt{n}(t-s) \begin{bmatrix} \widehat{VaR}_{[ns]:[nt]} - VaR \\ \widehat{ES}_{[ns]:[nt]} - ES \end{bmatrix} : (s, t) \in \Delta \right\} \quad (9)$$

converges in distribution in $\ell^\infty(\Delta) \times \ell^\infty(\Delta)$ to the process

$$\left\{ \Sigma^{1/2} \begin{bmatrix} W_1(t) - W_1(s) \\ W_2(t) - W_2(s) \end{bmatrix} : (s, t) \in \Delta \right\}, \quad (10)$$

where Σ is from Theorem 1, and W_1 and W_2 are independent standard Brownian motions.

3 Statistical Methods

3.1 Confidence Intervals

In time series analysis, confidence interval construction for an unknown quantity is often difficult, due to dependence. Indeed, from Theorem 1, we see that the standard errors appearing in the normal limiting distributions depend on the time series autocovariance at all integer lags. To construct confidence intervals using Theorem 1, these standard errors must be estimated. One approach, taken in Chen and Tang (2005); Chen (2008), is to estimate using kernel smoothing the spectral density at zero frequency of the transformed time series $g(X_1), g(X_2), \dots$ and $h(X_1), h(X_2), \dots$, where g and h are from Theorem 1. Although it is known that under certain moment and correlation assumptions, spectral density estimators are consistent for stationary processes (Brockwell and Davis, 1991; Anderson, 1971), in practice it is nontrivial to obtain robust and precise estimates

due to the need to select tuning parameters for the kernel smoothing-based approach. As for other approaches, under certain conditions, resampling methods such as the moving block bootstrap (Kunsch, 1989; Liu and Singh, 1992) and the subsampling method for time series (Politis et al., 1999) bypass direct standard error estimation and yield confidence intervals that asymptotically have the correct coverage probability. However, these approaches also require user-chosen tuning parameters such as the block length in the moving block bootstrap and the window width in subsampling. We introduce an alternative way to construct confidence intervals with asymptotically correct coverage, where the quality of the resulting confidence intervals is less sensitive to the choice of tuning parameters and is therefore more robust.

We first examine a technique called sectioning from the simulation literature (Asmussen and Glynn, 2007), which can be used to construct confidence intervals for general estimators. The method is as follows. Let $Y_1(\cdot), Y_2(\cdot), \dots$ be a sequence of random bounded real-valued functions on $[0, 1]$. For some user-specified integer $m \geq 2$, suppose we have the joint convergence in distribution:

$$\left(Y_n(1/m) - Y_n(0), Y_n(2/m) - Y_n(1/m), \dots, Y_n(1) - Y_n((m-1)/m) \right) \xrightarrow{d} \frac{\sigma}{m^{1/2}} \left(\mathcal{N}_1, \mathcal{N}_2, \dots, \mathcal{N}_m \right), \quad (11)$$

where $\sigma > 0$ and $\mathcal{N}_1, \dots, \mathcal{N}_m$ are independent standard normal random variables. Taking $Y_n(\cdot)$ to be the processes in (5) for VaR or ES, this is guaranteed by Theorem 1. Then, with

$$\begin{aligned} \bar{Y}_n &= m^{-1} \sum_{i=1}^m (Y_n(i/m) - Y_n((i-1)/m)) \\ S_n &= \left((m-1)^{-1} \sum_{i=1}^m (Y_n(i/m) - Y_n((i-1)/m) - \bar{Y}_n)^2 \right)^{1/2}, \end{aligned}$$

by the Continuous Mapping Theorem, as $n \rightarrow \infty$ with m fixed, $m^{1/2}\bar{Y}_n/S_n$ converges in distribution to the Student's t -distribution with $m-1$ degrees of freedom. So using the t -distribution critical values, we can obtain confidence intervals for VaR and ES with asymptotically correct coverage. Note that this method requires the number n/m to be sufficiently large for the asymptotic distribution in (11) to hold. Following Asmussen and Glynn (2007), we recommend selecting the integer m within the range of $[2, 10]$ in practice. In Section 4, we demonstrate through simulations that the sectioning method is very robust to choices of m within this range.

Next, we examine a generalization of sectioning, called self-normalization. This technique has been studied recently in the time series literature (Lobato, 2001; Shao, 2010), as well as earlier in the simulation literature, where it is known as standardization (Schruben, 1983; Glynn and Iglehart, 1990). As with sectioning, the method applies to confidence interval construction for general estimators. With self-normalization, the idea is to use a ratio-type statistic where the unknown standard error appears in both the numerator and the denominator and thus cancels, resulting in a pivotal limiting distribution. As before, let $Y_1(\cdot), Y_2(\cdot), \dots$ be a sequence of random bounded real-valued functions on $[0, 1]$. Suppose we have the distributional convergence in $D[0, 1]$: $Y_n(\cdot) \xrightarrow{d} \sigma W(\cdot)$, where $\sigma > 0$. Again, taking $Y_n(\cdot)$ to be the processes in (5) for VaR or ES,

this distributional convergence is guaranteed by Theorem 1. Consider some positive homogeneous functional $T : D[0, 1] \mapsto \mathbb{R}$, i.e., satisfying $T(\sigma Y) = \sigma T(Y)$ for $\sigma > 0$ and $Y \in D[0, 1]$. If the Continuous Mapping Theorem can applied, then

$$\frac{Y_n(1)}{T(Y_n)} \xrightarrow{d} \frac{W(1)}{T(W)}. \quad (12)$$

The right side of (12) is a pivotal limiting distribution. So using its critical values, which may be computed via simulation, we can obtain confidence intervals for VaR and ES with asymptotically correct coverage.

The choice of form for the functional T is up to the user. One convenient choice is $T(Y) = \left(\int_0^1 (Y(t) - tY(1))^2 dt\right)^{1/2}$, using which we obtain the following result for ES:

$$\frac{\widehat{ES}_n(p) - ES(p)}{\left(\int_0^1 t^2 (\widehat{ES}_{[nt]}(p) - \widehat{ES}_n(p))^2 dt\right)^{1/2}} \xrightarrow{d} \frac{W(1)}{(\int_0^1 (W(t) - tW(1))^2 dt)^{1/2}}. \quad (13)$$

This form for T , as advocated for by Lobato (2001), Shao (2010) and Shao and Zhang (2010) among others, ensures that the numerator and denominator of the right side of (13) are quantities based on independent normal random variables, which makes quantiles for their ratio particularly easy to compute.

3.2 Testing for a Single Change Point

As is the case with confidence interval construction with time series data, change-point testing in time series based on statistics constructed from functional central limit theorems and the continuous mapping theorem is often nontrivial due to the need to estimate standard errors. Motivated by the maximum likelihood method in the parametric setting, variants of the Page (1954) CUSUM statistic are commonly used for nonparametric change-point tests (Csorgo and Horvath, 1997), and generally rely on asymptotic approximations (via functional central limit theorems and the continuous mapping theorem) to supply critical values of pivotal limiting distributions under the null hypothesis of no change. As discussed in Vogelsang (1999); Shao and Zhang (2010); Zhang and Lavitas (2018), testing procedures where standard errors are estimated directly, for example, by estimating the spectral density of transformed time series via a kernel-smoothing approach, can be biased under the change-point alternative. Such bias can result in nonmonotonic power, i.e., power can decrease in some ranges as the alternative deviates from the null. To avoid this issue, Shao and Zhang (2010) and Zhang and Lavitas (2018) propose using self-normalization techniques to general change-point testing. We adopt this idea to our specific problem of detecting changes in tail risk measures.

As motivated in the Introduction (Section 1), it is important to perform hypothesis tests for abrupt changes of risk measures in the time series setting. We introduce the methodology for joint testing of VaR and ES. In this section, we consider the case of at most one change point. We consider the case of an unknown number of change points in the next section, using the approach in Zhang and Lavitas (2018). For a time series X_1, \dots, X_n , let (VaR_{X_i}, ES_{X_i}) be the VaR and ES

at a fixed level p for the marginal distribution of X_i . We test the following null and alternative hypotheses.

$$\mathcal{H}_0 : X_1, \dots, X_n \text{ is stationary, and in particular, } \begin{bmatrix} VaR_{X_1} \\ ES_{X_1} \end{bmatrix} = \dots = \begin{bmatrix} VaR_{X_n} \\ ES_{X_n} \end{bmatrix}.$$

\mathcal{H}_1 : There is $t^* \in (0, 1)$ such that

$$\begin{bmatrix} VaR_{X_1} \\ ES_{X_1} \end{bmatrix} = \dots = \begin{bmatrix} VaR_{X_{[nt^*]}} \\ ES_{X_{[nt^*]}} \end{bmatrix} \neq \begin{bmatrix} VaR_{X_{[nt^*]+1:n}} \\ ES_{X_{[nt^*]+1:n}} \end{bmatrix} = \dots = \begin{bmatrix} VaR_{X_n} \\ ES_{X_n} \end{bmatrix},$$

and $X_1, \dots, X_{[nt^*]}$ and $X_{[nt^*]+1}, \dots, X_n$ are separately stationary.

We base our change-point test on the following variant of the CUSUM process:

$$\left\{ \sqrt{nt}(1-t) \begin{bmatrix} \widehat{VaR}_{1:[nt]} - \widehat{VaR}_{[nt]+1:n} \\ \widehat{ES}_{1:[nt]} - \widehat{ES}_{[nt]+1:n} \end{bmatrix} : t \in [0, 1] \right\} \quad (14)$$

Note that we split the above process for all possible break points $t \in (0, 1)$ into a difference of two estimators, an estimator using $X_1, \dots, X_{[nt]}$ and an estimator using $X_{[nt]+1}, \dots, X_n$. Moreover, splitting the process as in (14) avoids potential VaR estimation using a sequence containing the change point, which could have undesirable behavior. In Proposition 2 below, we self-normalize the process in (4) using the approach of Shao and Zhang (2010). Note that the self-normalizer of (15) below takes into account the potential change point and is split into two separate integrals involving $X_1, \dots, X_{[nt]}$ and $X_{[nt]+1}, \dots, X_n$.

Proposition 2. Suppose Assumption 1 holds. Under the null hypothesis \mathcal{H}_0 ,

$$G_n := \sup_{t \in [0, 1]} C_n(t)^T D_n(t)^{-1} C_n(t), \quad (15)$$

with

$$C_n(t) := t(1-t) \begin{bmatrix} \widehat{VaR}_{1:[nt]} - \widehat{VaR}_{[nt]+1:n} \\ \widehat{ES}_{1:[nt]} - \widehat{ES}_{[nt]+1:n} \end{bmatrix}$$

$$D_n(t) := n^{-1} \sum_{i=1}^{[nt]} \left(\frac{i}{n} \right)^2 \begin{bmatrix} \widehat{VaR}_{1:i} - \widehat{VaR}_{1:[nt]} \\ \widehat{ES}_{1:i} - \widehat{ES}_{1:[nt]} \end{bmatrix}^{\otimes 2} + n^{-1} \sum_{i=[nt]+1}^n \left(\frac{n-i+1}{n} \right)^2 \begin{bmatrix} \widehat{VaR}_{i:n} - \widehat{VaR}_{[nt]+1:n} \\ \widehat{ES}_{i:n} - \widehat{ES}_{[nt]+1:n} \end{bmatrix}^{\otimes 2},$$

converges in distribution to

$$G := \sup_{t \in [0, 1]} C(t)^T D(t)^{-1} C(t), \quad (16)$$

with

$$C(t) := \begin{bmatrix} W_1(t) - tW_1(1) \\ W_2(t) - tW_2(1) \end{bmatrix}$$

$$D(t) := \int_0^t \begin{bmatrix} W_1(s) - \frac{s}{t}W_1(t) \\ W_2(s) - \frac{s}{t}W_2(t) \end{bmatrix}^{\otimes 2} ds + \int_t^1 \begin{bmatrix} W_1(1) - W_1(s) - \frac{1-s}{1-t}(W_1(1) - W_1(t)) \\ W_2(1) - W_2(s) - \frac{1-s}{1-t}(W_2(1) - W_2(t)) \end{bmatrix}^{\otimes 2} ds.$$

Assume the alternative hypothesis \mathcal{H}_1 is true with the change point occurring at some fixed (but unknown) $t^* \in (0, 1)$. For any fixed difference $VaR_{X_{[nt^*]}} = c_1 \neq c_2 = VaR_{X_{[nt^*]+1}}$ or $ES_{X_{[nt^*]}} = d_1 \neq d_2 = ES_{X_{[nt^*]+1}}$, we have $G_n \xrightarrow{P} \infty$ as $n \rightarrow \infty$. Furthermore, if the difference varies with n according to $c_1 - c_2 = n^{-1/2+\epsilon}L$ or $d_1 - d_2 = n^{-1/2+\epsilon}L$ for some $L \neq 0$ and $\epsilon \in (0, 1/2)$, then $G_n \xrightarrow{P} \infty$ as $n \rightarrow \infty$.

The distribution of G is pivotal, and its critical values may be obtained via simulation. For testing \mathcal{H}_0 versus \mathcal{H}_1 at some level, we reject \mathcal{H}_0 if the test statistic G_n exceeds some corresponding critical value of G . To obtain critical values, we simulate 5,000 replications, with each replication consisting of 2,000 independent standard normal random variables to approximate standard Brownian motions on $[0, 1]$.

In subsequent discussions concerning (15), we will refer to the process appearing in the numerator as the “CUSUM process”, the process appearing in the denominator as the “self-normalizer process”, and the entire ratio process as the “self-normalized CUSUM process”.⁵

3.3 Extension to Multiple Change Points

We extend our single change-point testing methodology to the case of multiple change points. Typically, the number of potential change points in the alternative hypothesis must be prespecified. However, we leverage the recent work of Zhang and Lavitas (2018) and introduce joint change-point tests for VaR and ES, that can accommodate an unknown, possibly multiple, number of change points in the alternative hypothesis. We fix some small $\delta > 0$ and consider the following null and alternative hypotheses (following the notation from Section 3.2).

$$\mathcal{H}_0 : X_1, \dots, X_n \text{ is stationary, and in particular, } \begin{bmatrix} VaR_{X_1} \\ ES_{X_1} \end{bmatrix} = \dots = \begin{bmatrix} VaR_{X_n} \\ ES_{X_n} \end{bmatrix}.$$

$$\mathcal{H}_1 : \text{There are } 0 = t_0^* < t_1^* < \dots < t_k^* < t_{k+1}^* = 1 \text{ with } t_j^* - t_{j-1}^* > \delta \text{ for } j = 1, \dots, k+1$$

$$\text{such that } \begin{bmatrix} VaR_{X_{[nt_j^*]}} \\ ES_{X_{[nt_j^*]}} \end{bmatrix} \neq \begin{bmatrix} VaR_{X_{[nt_j^*]+1}} \\ ES_{X_{[nt_j^*]+1}} \end{bmatrix}, \text{ and } X_{[nt_j^*]+1}, \dots, X_{[nt_{j+1}^*]} \text{ are separately stationary}$$

for $j = 0, \dots, k$.

Consider the index set $\Delta = \{(s, t) \in [\delta, 1-\delta]^2 : t-s \geq \delta\}$ and the test statistic

$$H_n = \sup_{(s_1, s_2) \in \Delta} E_n^f(s_1, s_2)^T F_n^f(s_1, s_2)^{-1} E_n^f(s_1, s_2) + \sup_{(t_1, t_2) \in \Delta} E_n^b(t_1, t_2)^T F_n^b(t_1, t_2)^{-1} E_n^b(t_1, t_2),$$

⁵To theoretically evaluate the efficiency of statistical tests, an analysis based on sequences of so-called local limiting alternatives (for example, sequences $c_1 - c_2 = O(n^{-1/2})$ in Proposition 2 above) can be considered (see, for example, van der Vaart (1998)). However, such an analysis would be considerably involved, and we leave it for future study.

where

$$\begin{aligned}
E_n^f(s_1, s_2) &= \frac{[ns_1]([ns_2] - [ns_1])}{[ns_2]^{3/2}} \left[\frac{\widehat{VaR}_{1:[ns_1]} - \widehat{VaR}_{[ns_1]+1:[ns_2]}}{\widehat{ES}_{1:[ns_1]} - \widehat{ES}_{[ns_1]+1:[ns_2]}} \right] \\
F_n^f(s_1, s_2) &= \sum_{i=1}^{[ns_1]} \frac{i^2([ns_1] - i)^2}{[ns_2]^2[ns_1]^2} \left[\frac{\widehat{VaR}_{1:i} - \widehat{VaR}_{i+1:[ns_1]}}{\widehat{ES}_{1:i} - \widehat{ES}_{i+1:[ns_1]}} \right]^{\otimes 2} \\
&\quad + \sum_{i=[ns_1]+1}^{[ns_2]} \frac{(i-1-[ns_1])^2([ns_2]-i+1)^2}{[ns_2]^2([ns_2]-[ns_1])^2} \left[\frac{\widehat{VaR}_{[ns_1]+1:i-1} - \widehat{VaR}_{i:[ns_2]}}{\widehat{ES}_{[ns_1]+1:i-1} - \widehat{ES}_{i:[ns_2]}} \right]^{\otimes 2} \\
E_n^b(t_1, t_2) &= \frac{([nt_2] - [nt_1])(n - [nt_2] + 1)}{(n - [nt_1] + 1)^{3/2}} \left[\frac{\widehat{VaR}_{[nt_2]:n} - \widehat{VaR}_{[nt_1]:[nt_2]-1}}{\widehat{ES}_{[nt_2]:n} - \widehat{ES}_{[nt_1]:[nt_2]-1}} \right] \\
F_n^b(t_1, t_2) &= \sum_{i=[nt_1]}^{[nt_2]-1} \frac{(i - [nt_1] + 1)^2([nt_2] - 1 - i)^2}{(n - [nt_1] + 1)^2([nt_2] - [nt_1])^2} \left[\frac{\widehat{VaR}_{[nt_1]:i} - \widehat{VaR}_{i+1:[nt_2]-1}}{\widehat{ES}_{[nt_1]:i} - \widehat{ES}_{i+1:[nt_2]-1}} \right]^{\otimes 2} \\
&\quad + \sum_{i=[nt_2]}^n \frac{(i - [nt_2])^2(n - i + 1)^2}{(n - [nt_1] + 1)^2(n - [nt_2] - 1)^2} \left[\frac{\widehat{VaR}_{i:n} - \widehat{VaR}_{[nt_2]:i-1}}{\widehat{ES}_{i:n} - \widehat{ES}_{[nt_2]:i-1}} \right]^{\otimes 2}.
\end{aligned}$$

Then, under \mathcal{H}_0 , applying Theorem 3 of Zhang and Lavitas (2018), our Theorem 2 above yields the following result.

Corollary 1. Suppose Assumption 1 holds. Under the null hypothesis \mathcal{H}_0 ,

$$\begin{aligned}
H_n &\xrightarrow{d} \sup_{(s_1, s_2) \in \Delta} E(0, s_1, s_2)^T F(0, s_1, s_2)^{-1} E(0, s_1, s_2) + \sup_{(t_1, t_2) \in \Delta} E(t_1, t_2, 1)^T F(t_1, t_2, 1)^{-1} E(t_1, t_2, 1) \\
&:= H,
\end{aligned}$$

where

$$\begin{aligned}
E(r_1, r_2, r_3) &= \begin{bmatrix} W_1(r_2) - W_1(r_1) - \frac{r_2 - r_1}{r_3 - r_1} (W_1(r_3) - W_1(r_1)) \\ W_2(r_2) - W_2(r_1) - \frac{r_2 - r_1}{r_3 - r_1} (W_2(r_3) - W_2(r_1)) \end{bmatrix} \\
F(r_1, r_2, r_3) &= \int_{r_1}^{r_2} \begin{bmatrix} W_1(s) - W_1(r_1) - \frac{s - r_1}{r_2 - r_1} (W_1(r_2) - W_1(r_1)) \\ W_2(s) - W_2(r_1) - \frac{s - r_1}{r_2 - r_1} (W_2(r_2) - W_2(r_1)) \end{bmatrix}^{\otimes 2} ds \\
&\quad + \int_{r_2}^{r_3} \begin{bmatrix} W_1(r_3) - W_1(s) - \frac{r_3 - s}{r_3 - r_2} (W_1(r_3) - W_1(r_2)) \\ W_2(r_3) - W_2(s) - \frac{r_3 - s}{r_3 - r_2} (W_2(r_3) - W_2(r_2)) \end{bmatrix}^{\otimes 2} ds.
\end{aligned}$$

Under the alternative \mathcal{H}_1 , $H_n \xrightarrow{P} \infty$ as $n \rightarrow \infty$.

To reduce the computational burden of the method, we use a grid approximation suggested by Zhang and Lavitas (2018), where in the doubly-indexed set Δ , one index is reduced to a coarser

grid. Specifically, let $\mathcal{G}_\delta = \{(1 + k\delta)/2 : k \in \mathbb{Z}\} \cap [0, 1]$ and consider the modified statistic

$$\begin{aligned}\tilde{H}_n &= \sup_{(s_1, s_2) \in \Delta \cap ([0, 1] \times \mathcal{G}_\delta)} E_n^f(s_1, s_2)^T F_n^f(s_1, s_2)^{-1} E_n^f(s_1, s_2) \\ &\quad + \sup_{(t_1, t_2) \in \Delta \cap (\mathcal{G}_\delta \times [0, 1])} E_n^b(t_1, t_2)^T F_n^b(t_1, t_2)^{-1} E_n^b(t_1, t_2).\end{aligned}\tag{17}$$

As before, under \mathcal{H}_0 , we have

$$\begin{aligned}\tilde{H}_n &\xrightarrow{d} \sup_{(s_1, s_2) \in \Delta \cap ([0, 1] \times \mathcal{G}_\delta)} E(0, s_1, s_2)^T F(0, s_1, s_2)^{-1} E(0, s_1, s_2) \\ &\quad + \sup_{(t_1, t_2) \in \Delta \cap (\mathcal{G}_\delta \times [0, 1])} E(t_1, t_2, 1)^T F(t_1, t_2, 1)^{-1} E(t_1, t_2, 1) \\ &:= \tilde{H}.\end{aligned}\tag{18}$$

Note that simply using the original doubly-indexed set Δ , for a sample of size n and an arbitrary number of change points, we would need to search for maxima over $O(n^2)$ points. However, using the grid approximation, we need only search for maxima over $O(n)$ points. In contrast, if we were to use a direct extension of the single-change point detection methodology of Section 3.2, with m change points (which needs to be specified in advance), we would need to search for maxima over $O(n^m)$ points. Hence, the methodology introduced in this section offers significant computational savings.

We reject \mathcal{H}_0 if \tilde{H}_n exceeds the critical value corresponding to a desired test level of the pivotal quantity \tilde{H} . To obtain critical values, we simulate 10,000 replications, with each replication consisting of 5,000 independent standard normal random variables to approximate standard Brownian motion on $[0, 1]$.

4 Simulations

We perform an extensive simulation study to investigate the finite-sample performance of ES confidence interval construction using the sectioning and self-normalization methods (Section 3.1) as well as upper tail change detection (Sections 3.2 and 3.3) using ES. Our simulations are based on a widely used and practically relevant data-generating process for modeling financial time series, namely Generalized Autoregressive Conditional Heteroskedasticity (GARCH) models. Specifically, in the main text we consider

$$\begin{aligned}X_i &= \sigma_i \epsilon_i, \\ \sigma_i^2 &= \omega + \lambda_1 X_{i-1}^2 + \lambda_2 \sigma_{i-1}^2,\end{aligned}$$

where the conditional variance σ_i^2 follows a GARCH(1,1) process. The innovations ϵ_i are assumed to be i.i.d. standard normal, and the model parameters are set as $\omega = 0.01$, $\lambda_1 = 0.1$, and $\lambda_2 = 0.8$. This parameterization yields a highly persistent yet stationary process, as $\lambda_1 + \lambda_2$ approaches 1. Our choice of parameters follows Bollerslev (1986), where these parameters are estimated for

a GARCH(1,1) model on lower-frequency financial time series data.⁶ The Appendix collects a comprehensive set of robustness results with different parameters for the GARCH model and t -distributed innovations. In particular, in Figure A.1 we also show the results for a more persistent GARCH(1,1) process with parameters $\omega = 0.01$, $\lambda_1 = 0.1$, and $\lambda_2 = 0.9$, which better reflects the dynamics of higher-frequency financial return series. This choice of λ_1 and λ_2 is also adopted in the recent paper Horváth et al. (2024). All our results are robust to these parameter choices.

4.1 Confidence Intervals

We begin by studying how the empirical coverage probability of confidence intervals depends on the sample size. In Figure 1, we vary the time series sample size from 200 to 3,000 and examine the widths and empirical coverage probabilities of the 95% confidence intervals for ES in the upper 5th percentile. These confidence intervals are constructed using the sectioning and self-normalization methods (Section 3.1) for the GARCH(1,1) process introduced above. For comparison, we also include confidence intervals constructed using the block bootstrap method, as described in Bühlmann (2002).

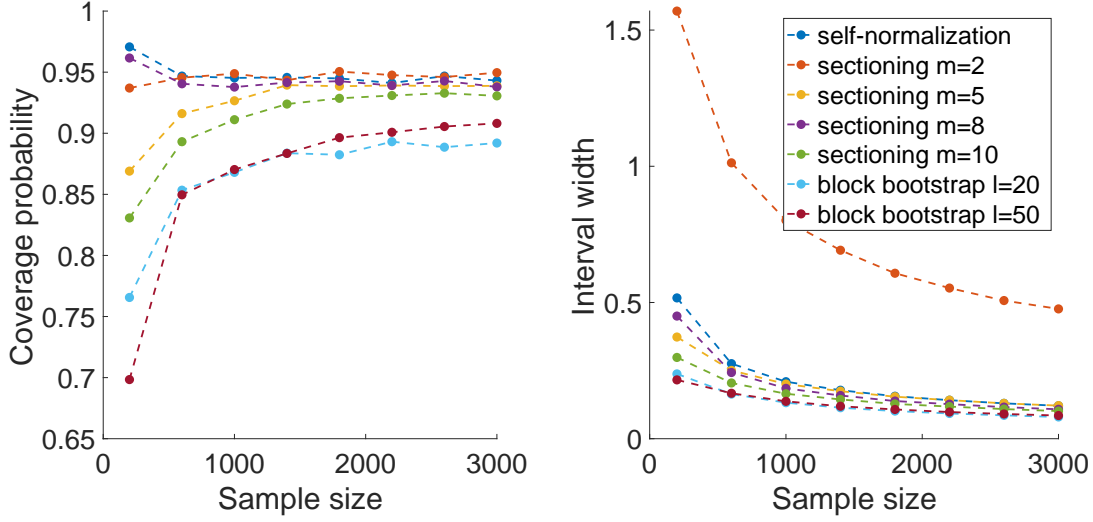
For the sectioning method, we show that the results are robust to the sectioning parameter m . We study the coverage probability and confidence intervals for the sectioning parameter $m \in \{2, 5, 8, 10\}$. For the self-normalization method, we use the functional $T(Y)$ defined as $T(Y) = (\int_0^1 (Y(t) - tY(1))^2 dt)^{1/2}$, as recommended in Section 3.1. The block bootstrap method is applied with block lengths $l \in \{20, 50\}$, and for this method, confidence intervals are constructed using the 0.025 and 0.975 quantiles of its empirical distribution. We average the estimates run over 10,000 replications. For each replication, we use a burn-in period of 5,000 to ensure the GARCH(1,1) process approximately reaches stationarity. Appendix B collects a comprehensive set of additional robustness results that confirm our findings. We repeat the simulation study for GARCH (1,1) models with parameters $\lambda_2 \in \{0.5, 0.6, 0.7, 0.8\}$ and t -distributed innovations ϵ_i with degrees of freedom $\nu = 15$.

Figure 1 shows that both the self-normalization method and sectioning method with different parameters m achieve good coverage when the sample size is large. In particular, the coverage probability of the confidence intervals constructed by the sectioning method is robust to different choices of $m \in [2, 10]$. In contrast, the block bootstrap method yields lower coverage probabilities and performs worse than our proposed methods, requiring larger sample sizes to approximate the nominal coverage rate. Additionally, the block bootstrap is also sensitive to the choice of the block length. Furthermore, the sectioning method with a larger $m \in \{5, 8, 10\}$ produces smaller confidence intervals, but generally yields lower empirical coverage probabilities compared to the self-normalization method. This is especially pronounced for small sample sizes such as 200 or 500.⁷ As the sample size increases, the performance of the two methods becomes more similar, and the desired coverage probability of 0.95 is approximately reached. While choosing $m = 2$ in the

⁶Bollerslev (1986) estimates the parameters $(\omega, \lambda_1, \lambda_2) = (0.007, 0.135, 0.829)$ using quarterly U.S. inflation data from February 1948 to April 1983. While these parameters are not calibrated based on high-frequency asset returns, they are widely cited in the literature and serve as a benchmark for evaluating model performance.

⁷While a sample size of 200 or 500 is statistically small, obtaining such samples at lower frequencies (e.g., quarterly data) requires a long time span.

Figure 1: Coverage Probability and Confidence Interval Width for Different Sample Sizes



This figure shows the coverage probability and confidence interval width for different sample size. We use the GARCH(1,1) process with i.i.d. standard normal innovations, and set the model parameters as $\omega = 0.01$, $\lambda_1 = 0.1$, and $\lambda_2 = 0.8$. Left subfigure: relationship between sample size and empirical coverage probability of 95% confidence intervals for ES in the upper 5th percentile computed for stationary GARCH(1,1) process. Right subfigure: relationship between time series sample size and width of 95% confidence intervals for ES in the upper 5th percentile computed for a stationary GARCH(1,1) process. Each plotted point is the averaged result over 10,000 replications.

sectioning method can lead to wider confidence intervals, this can be easily identified in practice, allowing for the selection of a larger m that leads to a tighter interval width.

4.2 Detection of Location Change in Tail

We investigate through simulations the detection of abrupt location changes using ES in the upper 5th percentile, as discussed in Section 3.2. To assess the robustness of our method in detecting change points at different locations within the time series, we consider changes occurring at $t = rT$ with $r \in \{0.5, 0.6, 0.7, 0.8, 0.9\}$, where T is the time horizon.

We consider the GARCH(1,1) process introduced previously before the potential distribution change at time $t = rT$. After the change point, we consider the following process, where the magnitude μ of the location change varies between 0 (the null hypothesis of no change) and 1, that is, $\mu \in [0, 1]$:

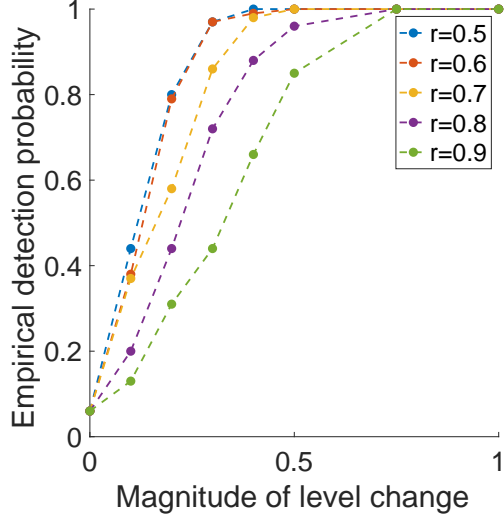
$$X_i = \mu + \sigma_i \epsilon_i,$$

$$\sigma_i^2 = 0.01 + 0.1(X_{i-1} - \mu)^2 + 0.8\sigma_{i-1}^2.$$

Figure 2 shows the approximate power of change-point tests using the self-normalized CUSUM statistic (see (15)-(16)) at the 0.05 significance level for varying magnitudes of the abrupt location change. For each data point, we perform 100 replications of the change-point testing using time series sequences of length 2,000. For each replication, we use a burn-in period of 5,000 to ensure the GARCH(1,1) process approximately reaches stationarity.

As expected, the power of the test increases monotonically with the magnitude of the location

Figure 2: Empirical Detection Probability for Different Magnitudes of Changes



This figure shows the relationship between the empirical detection probability and magnitude of location change in the mean for change point detection with 0.05 significance level using ES in the upper 5th percentile. The abrupt location change occurs at $t = rT$ with $r \in \{0.5, 0.6, 0.7, 0.8, 0.9\}$ of the time series sequence. The magnitude of the change in the mean is in the interval $[0, 1]$. Each plotted point is the average over 100 replications with time series sequences of length 2,000 in each replication.

change. In accordance with the desired 0.05 significance level of our procedure, the probability of false positive detection is approximately 0.05, as indicated by the points with zero magnitude of location change in Figure 2. While the location of the change point does affect the detection probability, the test is robust when the change occurs between the $r = 0.5$ and 0.8 fractions of the series. For changes occurring at the very end of the series (at $r = 0.9$), the detection probability decreases. However, the test can still achieve high detection power as the magnitude of the change increases.

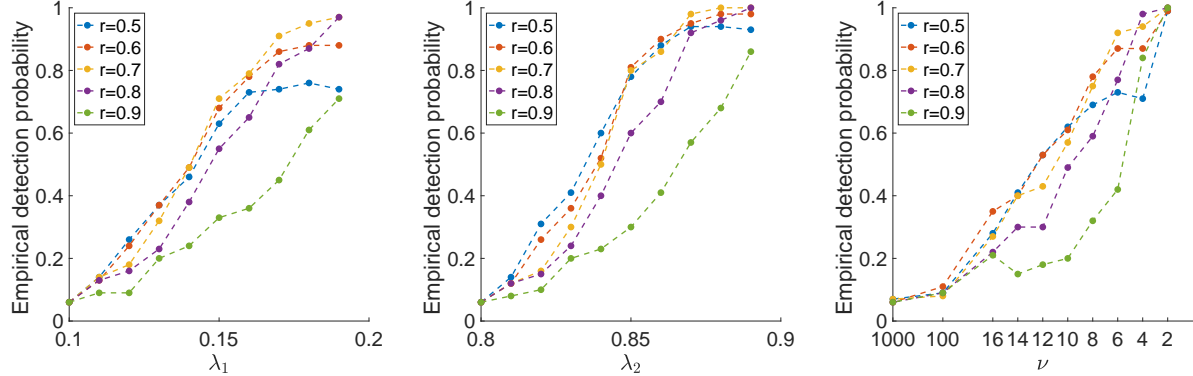
While our method can detect changes in the mean, it is specifically designed to capture more general changes in the distribution. Therefore, when the change occurs solely in the mean, our method may require a relatively larger magnitude of shift for detection compared to methods designed specifically for mean change detection. In the next section, we focus on more complex structural breaks, where our method is particularly useful and demonstrates strong performance.

4.3 Detection of General Change in Tail

We also investigate the detection of general structural changes in the upper tail of the underlying marginal distribution occurring at different points within the time interval. Although the relationship between power and the “magnitude” of the change in the upper tail is not as simple as in the case of pure location change, nevertheless, with Proposition 2 we will detect the change with high probability as our sample size increases. In our simulations, we study the detection of general structural changes in the tail using ES in the upper 5th percentile, as discussed in Section 3.2.

As in the previous section, we consider the GARCH(1,1) process with i.i.d. normal innovations and parameters $\omega = 0.01$, $\lambda_1 = 0.1$, and $\lambda_2 = 0.8$ before the distribution change at time $t = rT$,

Figure 3: Empirical Detection Probability for Different Changes in Tail Parameters



This figure shows the empirical detection probability for different changes in parameters that affect the tail behavior. Left subfigure: change-point tests for setup 1. Relationship between empirical detection probability and λ_1 after the change point at $t = rT$. Before the change point, $\lambda_1 = 0.1$. Middle subfigure: change-point tests for setup 2. Relationship between empirical detection probability and λ_2 after the change point at $t = rT$. Before the change point, $\lambda_2 = 0.8$. Right subfigure: change-point tests for setup 3. Relationship between empirical detection probability and the degrees of freedom ν in $t(\nu)$ -distributed innovations after the change point at $t = rT$. Before the change point, the innovations are standard normal distributed. In all cases, change-point testing is conducted with a 0.05 significance level using ES in the upper 5th percentile. Each plotted point is an average over 100 replications using time series sequences of length 2,000.

with $r = \{0.5, 0.6, 0.7, 0.8, 0.9\}$. After the change point, we consider the following processes:

- (1) $X_i = \sigma_i \epsilon_i$, $\sigma_i^2 = 0.01 + \lambda_1 X_{i-1}^2 + 0.8 \sigma_{i-1}^2$, $\epsilon_i \stackrel{i.i.d.}{\sim} \mathcal{N}(0, 1)$;
- (2) $X_i = \sigma_i \epsilon_i$, $\sigma_i^2 = 0.01 + 0.1 X_{i-1}^2 + \lambda_2 \sigma_{i-1}^2$, $\epsilon_i \stackrel{i.i.d.}{\sim} \mathcal{N}(0, 1)$;
- (3) $X_i = \sigma_i \epsilon_i$, $\sigma_i^2 = 0.01 + 0.1 X_{i-1}^2 + 0.8 \sigma_{i-1}^2$, $\epsilon_i \stackrel{i.i.d.}{\sim} t(\nu)$.

In the first setup, we vary the persistence parameter λ_1 from 0.1 to 0.19. In the second setup, we vary the parameter λ_2 from 0.8 to 0.89. These ranges of parameters ensure that the process remains stationary. In the last setup, we consider a change in the heavy-tailedness of the underlying distribution, transitioning from Gaussian innovations to t -distributed innovations with degrees of freedom $\nu \in \{2, 4, 6, 8, 10, 12, 14, 16, 100, 1000\}$. As ν increases, the t -distribution approaches the Gaussian distribution, and hence we expect the detection probability to decline accordingly. Figure 3 shows the approximate power of change-point tests using the self-normalized CUSUM statistic (see (15)) at the 0.05 significance level. For each data point, we perform 100 replications using times series sequences of length 2,000 and use an initial burn-in period of 5,000 to approximately reach stationarity.

As expected, for all types of changes, the power is approximately a monotonic function of the magnitude of change. Furthermore, our method is generally robust to the location of the change point, provided that it is not located near the very end of the time period. When the change point occurs close to the end of the series, the detection probability decreases slightly, but our method is still able to detect the change with high probability as the magnitude of the change increases.

4.4 Detection of Multiple Changes in Tail

We additionally investigate the detection of multiple structural changes in the upper tail of the underlying marginal distribution. Here, we again use ES in the upper 5th percentile and compare the practical performance of the single change-point methodology discussed in Section 3.2 with the unsupervised multiple change-point methodology discussed in Section 3.3. We consider the following variant of the GARCH(1,1) process introduced previously:

$$\text{GARCH}(1,1) \text{ process: } X_i = \begin{cases} \sigma_i \epsilon_i, \epsilon_i \stackrel{i.i.d.}{\sim} N(0, 1) & \text{for } i \leq [n/3] \\ \sigma_i u_i, u_i \stackrel{i.i.d.}{\sim} t(\nu) & \text{for } [n/3] \leq i \leq [2n/3], \\ \sigma_i \epsilon_i, \epsilon_i \stackrel{i.i.d.}{\sim} N(0, 1) & \text{for } i \geq [2n/3] \end{cases} \quad (19)$$

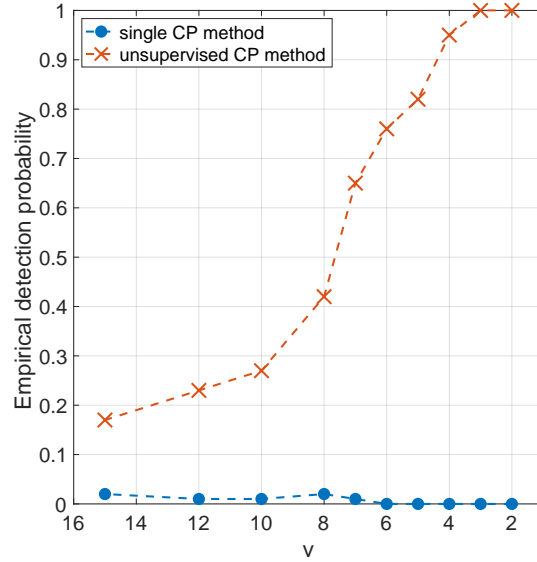
$$\sigma_i^2 = 0.01 + 0.1X_{i-1}^2 + 0.8\sigma_{i-1}^2.$$

In this GARCH(1,1) process, the innovations initially have relatively light tails, then change to heavier tails with $t(\nu)$ -distributed innovations, and finally revert back to the original lighter tails.

Figure 4 shows the approximate detection power of at least one change point as ν varies using the single change-point methodology (see (15)-(16)) versus the unsupervised multiple change-point methodology (see (17)-(18)) at the 0.05 significance level. For each data point, we perform 100 replications using time series sequences of length 1,200. For each replication, we use an initial burn-in period of 5,000 to approximately reach stationarity in the GARCH(1,1) process.

We observe that the single change-point testing method is unable to detect a change in the process in (19), even for extremely strong deviations from the null such as the case $\nu = 2$. In fact,

Figure 4: Comparison between Unsupervised Multiple and Single Change-Point Tests



This figure compares unsupervised multiple change-point tests with single change-point tests at the 0.05 significance level using ES in the upper 5th percentile. We plot the relationship between the empirical detection probability of at least one change point and the degrees of freedom ν of t-distributed innovations. Each plotted point is an average over 100 replications using time series sequences of length 1,200.

its power decays to zero as the magnitude of the change increases. This occurs because the single change-point test assumes that only one change point occurs and seeks to divide the time series into two sections separated by a single change point. Consequently, the effects of multiple changes can be “canceled out”. On the other hand, the unsupervised multiple change-point test exhibits the desired performance with increasing power as the magnitude of the change increases. Hence, it is a promising candidate for detecting more complex patterns of changes in the tails of time series.

5 Empirical Applications

5.1 Data and Expected Shortfall Estimation

We study the changes in tail risk for two of the most important macroeconomic indicators that reflect the conditions in the U.S. stock market and for interest rates. First, we consider the daily log returns of the S&P 500 Index, which is a proxy for a market risk factor, for the years 1928-2023.⁸ Second, we analyze the weekly log returns of U.S. 1-year and 10-year zero-coupon bonds for the years 1961-2023. We obtain the data from the U.S. Treasury Discount Bond Database provided by Filipovic et al. (2022), which is shown to provide the most reliable estimates. These bonds are tradable portfolios of U.S. Treasuries and reflect information in interest rates.

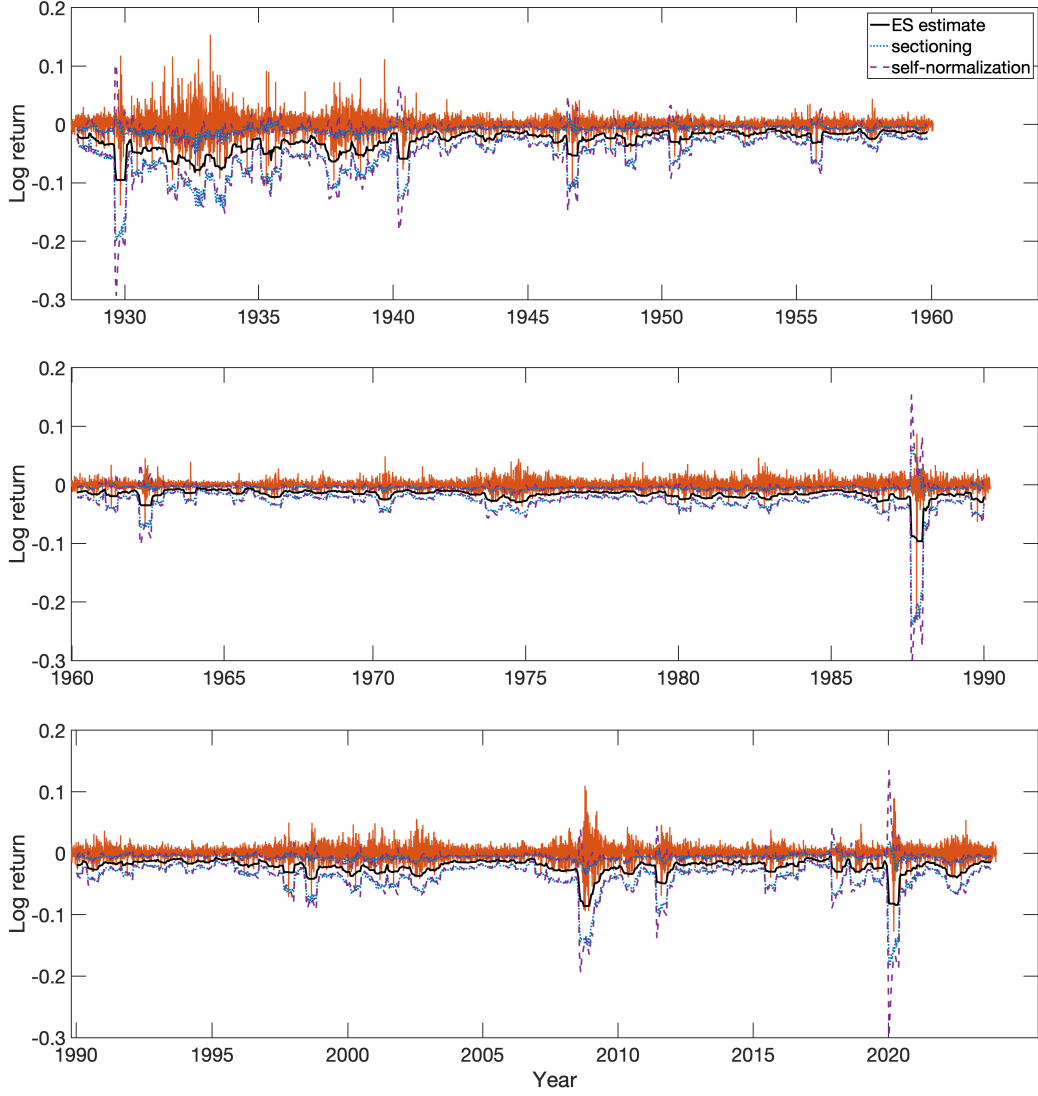
We begin our study with an analysis of the expected shortfall (ES) over time. We first apply the two methods of confidence interval construction from Section 3.1 to the daily log returns of S&P 500 for the period from January 03, 1928 to December 29, 2023. In Figure 5, we show ES estimates of the lower 5th percentile of log returns throughout this time period along with 95% confidence bands computed using the sectioning and self-normalization methods. We use the sectioning method with $m = 10$. (Our simulation study demonstrates that the coverage results are robust to the choices of the tuning parameter m .) We use a rolling window of 100 days with 90 days of overlap between successive windows. The self-normalization method appears to be more conservative and yields a wider confidence band compared to the sectioning method, which agrees with the results presented in Figure 1. Overall, the ES estimates and confidence bands appear to capture well the increased volatility of returns during periods of financial instability, such as the 1929 Wall Street Crash, World War II in 1940, the 1987 Black Monday Crash, the 2008 Financial Crisis, and the COVID-19 Pandemic in 2020.

We next apply the two methods of confidence interval construction from Section 3.1 to weekly log returns of U.S. 1-year and 10-year zero-coupon bonds for the period from July 03, 1961 to August 31, 2023. In Figure 6, we show ES estimates of the lower 10th percentile of log returns throughout this time period along with 95% confidence bands computed using the sectioning and self-normalization methods. We use a rolling window of 40 weeks with 30 weeks of overlap between successive windows. Again, the self-normalization method appears to be more conservative and yields a wider confidence band compared to the sectioning method. Although time series for bond returns have a greater degree of autocorrelation compared to S&P 500 returns, our methods are still applicable.⁹

⁸We obtain the time-series from Yahoo Finance.

⁹For comparison, we also estimate the ES with a parametric GARCH(1,1) model. Figures A.17 and A.18 in the

Figure 5: Expected Shortfall of Market Returns over Time

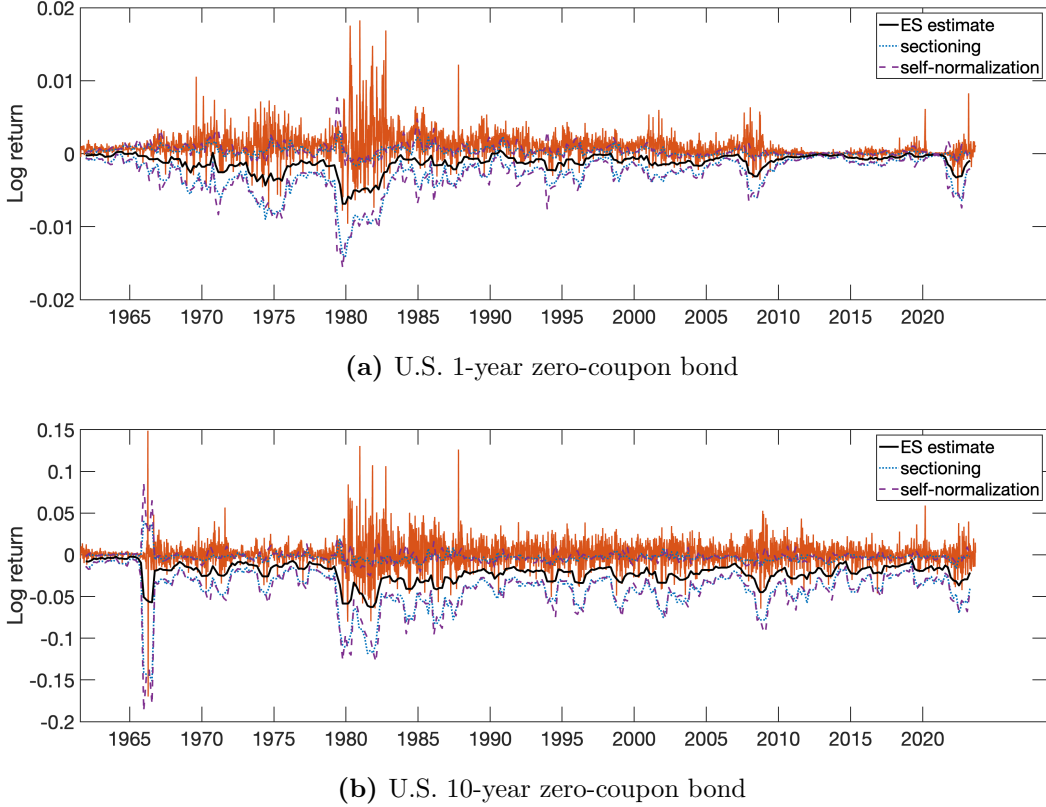


This figure shows the daily log returns and expected shortfall with confidence intervals for the S&P 500 index that approximates a market return time-series. We plot the ES estimate and 95% confidence bands for the lower 5th percentile. ES is computed using a rolling window of 100 days with 10 day shifts.

These rolling window estimates of ES with confidence intervals provide a valuable tool to get insight into the variation of the tail behavior of these time series. However, they are not a formal test for change points. Such tests are based on our novel statistics, which we study next.

Appendix collect the results. We show that for both the S&P 500 log returns and U.S. 10-year bond log returns, the ES estimates are broadly similar using the parametric GARCH model and our method. However, the parametric GARCH model can lead to unstable and spurious results. For example, for the U.S. 1-year bond log returns, the ES estimates show some noticeable differences, indicating that our method and the parametric model can yield different results. The estimation of the GARCH model on a rolling window can also lead to issues, and on approximately 10% of the rolling windows the optimizer failed to converge. For example, for the period from March 3, 1930 to July 23, 1930, the optimization method failed for both GARCH(1,1) models with either t -distributed innovations or normal innovations. We only plot the ES estimates from the GARCH model when the fitting process succeeds. Overall, our method appears to be more robust and reliable.

Figure 6: Expected Shortfall of Bond Returns over Time



This figure shows the weekly log returns and expected shortfall with confidence intervals for long- and short-maturity zero-coupon bonds. We plot the ES estimate and 95% confidence bands for the lower 10th percentile of log returns. ES is computed using a rolling window of 40 weeks with 10 week shifts.

5.2 Change-Point Detection

We now apply our change-point testing methodology to the equity and bond return time-series. We use our single and multiple change-point testing methodology for ES of the lower 5th percentile of S&P 500 daily log returns and of the lower 10th percentile of U.S. 1-year and 10-year zero-coupon bonds weekly log returns. For a systematic study, we run the tests on rolling windows over the full return time series. We compare the behavior of the tests and also visualize the return time-series on windows of interest.¹⁰

In more detail, we apply our single (based on (15)-(16)) and multiple (based on (17)-(18)) change-point tests to S&P 500 returns in successive 6-month and 1-year time windows, with 1 month of shift between successive windows. In Figures A.9-A.12 in Appendix C, we plot the test statistics for single and multiple change-point tests for ES in the lower 5th percentile of S&P 500 log returns for different time windows. We also indicate the critical value for the 0.05 significance

¹⁰Recall that our change-point testing methodology is meant to test for change(s) in a *given* time window, and help assess whether or not risk measures are stationary over the window. For the rolling window demonstrations in this section, if one is interested in performing statistical inference simultaneously for all windows, then one could run a multiple hypothesis testing procedure that controls the False Discovery Rate (FDR). A robust (albeit conservative) choice of procedure, which is valid for arbitrary dependence among the tests, is the Benjamini-Yekutieli (B-Y) procedure (Benjamini and Yekutieli, 2001). A description of the B-Y procedure is provided at the end of Appendix C.

Table 1: Examples of Change-Point Tests for S&P 500 Returns

time window	single CP test		multiple CP test	
	statistic	p-value	statistic	p-value
01/02/1929 - 12/31/1929	64.0	0.018	226.8	0.004
12/01/1939 - 05/31/1940	157.3	0.001	387.6	<0.001
06/01/1939 - 05/31/1940	43.2	0.045	328.2	<0.001
06/03/1946 - 11/29/1946	58.6	0.023	155.0	0.029
02/01/1950 - 07/31/1950	77.0	0.008	241.2	0.003
08/01/1957 - 07/31/1958	66.8	0.015	199.6	0.010
08/01/1962 - 07/31/1963	62.7	0.020	149.7	0.035
08/01/1969 - 07/31/1970	69.7	0.014	168.6	0.020
05/01/1987 - 10/30/1987	142.0	0.001	167.5	0.021
01/02/1987 - 12/31/1987	41.7	0.049	216.8	0.006
05/01/2008 - 10/31/2008	72.6	0.011	186.6	0.012
09/01/2017 - 02/28/2018	245.1	<0.001	306.1	0.001
10/01/2019 - 03/31/2020	130.4	0.001	276.4	0.001
11/01/1963 - 04/30/1964	58.5	0.023	119.6	0.085
10/02/2006 - 03/30/2007	73.9	0.010	99.1	0.156
03/01/2011 - 08/31/2011	80.8	0.007	132.8	0.059
04/01/1955 - 03/29/1956	7.3	0.514	177.3	0.016
05/01/2008 - 04/30/2009	8.0	0.487	171.7	0.018
09/03/2019 - 08/31/2020	4.6	0.702	220.4	0.005

This table shows results for single and multiple change-point tests for expected shortfall (ES) in the lower 5th percentile for S&P 500 daily log returns in different time windows. We report the change-point test statistics and the corresponding p-values. The top blocks show examples of where both the single and multiple change-point tests are significant. The middle blocks show examples of where the single change-point test is significant, but the multiple change-point test is not. The lower blocks show examples of where the multiple change-point test is significant, but the single change-point test is not.

level. Then, we apply the two change-point tests to weekly log returns of the zero-coupon bonds. We use successive 5-year and 10-year time windows for both bonds, with 3 months of shift between successive windows. In Figures A.13-A.16 in Appendix C, we plot the test statistics for single and multiple change-point tests for ES in the lower 10th percentile of U.S. 1-year and 10-year zero-coupon bond log returns for different time windows.

In Tables 1 and 2, for S&P 500 returns and bond returns, respectively, we report examples of the single and multiple change-point test results. For each window, we report the test statistics and the corresponding p-values.¹¹

There are examples of time windows where both the single and multiple change-point tests detect change at the 0.05 significance level. We collect some of these examples in the top block of Tables 1 and 2. To gain better intuition for the results, we also plot the return time series for some of these examples. In Figure 7, we plot the return time series for the S&P 500 log returns for periods including major events such as the 1929 Wall Street Crash, World War II in 1940, the

¹¹In Table A.1, we also report results from applying the B-Y multiple hypothesis testing adjustment for single and multiple change-point tests over rolling windows for the bond returns. Despite the conservativeness of the B-Y procedure, the bond returns generally exhibit less volatility relative to the S&P 500 returns, and allow for discoveries with FDR control. Unfortunately, the B-Y procedure is too conservative to reliably make discoveries with FDR control for S&P 500 returns.

Table 2: Examples of Change-Point Tests for Bond Returns

time window	single CP test		multiple CP test	
	statistic	p-value	statistic	p-value
US 1-year bond weekly log returns				
10/18/1961 - 09/19/1971	104.5	0.002	173.5	0.018
06/24/1973 - 06/11/1978	107.9	0.002	172.3	0.018
06/20/1976 - 06/07/1981	253.1	<0.001	350.4	<0.001
06/15/1980 - 06/02/1985	244.3	<0.001	293.3	0.001
12/16/1979 - 11/26/1989	418.1	<0.001	492.4	<0.001
08/12/2007 - 07/29/2012	98.2	0.003	180.1	0.015
08/05/2012 - 07/23/2017	155.1	0.001	290.0	0.001
02/03/2013 - 01/15/2023	93.3	0.004	339.0	<0.001
01/28/2018 - 01/15/2023	151.3	0.001	328.9	<0.001
10/06/1963 - 09/22/1968	65.3	0.016	87.4	0.222
11/22/1998 - 11/09/2003	84.9	0.005	84.1	0.246
04/30/2017 - 04/17/2022	94.1	0.003	124.4	0.075
08/14/2005 - 08/01/2010	7.1	0.524	188.1	0.012
09/19/1976 - 08/31/1986	5.0	0.671	477.8	<0.001
11/23/1997 - 11/04/2007	2.8	0.924	162.4	0.024
11/14/2004 - 10/26/2014	9.1	0.433	189.1	0.012
11/06/2011 - 10/17/2021	2.4	0.978	228.0	0.004
US 10-year bond weekly log returns				
12/26/1971 - 12/06/1981	471.5	<0.001	542.3	<0.001
06/20/1976 - 06/07/1981	281.0	<0.001	362.0	<0.001
06/17/1979 - 05/28/1989	47.1	0.039	151.4	0.033
06/12/1983 - 05/23/1993	222.5	0.001	354.1	<0.001
08/15/2004 - 08/02/2009	105.7	0.002	159.7	0.025
01/28/2018 - 01/15/2023	106.3	0.002	203.9	0.008
01/06/1963 - 12/24/1967	144.3	0.001	96.7	0.168
09/14/1980 - 09/01/1985	58.6	0.023	127.3	0.068
11/17/2002 - 11/04/2007	77.4	0.008	106.6	0.128
07/29/2018 - 07/16/2023	68.6	0.014	127.2	0.069
12/18/1977 - 11/29/1987	3.2	0.874	233.0	0.004
12/14/1980 - 11/25/1990	16.8	0.237	171.7	0.018
11/19/2000 - 10/31/2010	2.9	0.916	162.6	0.024

This table shows results for single and multiple change-point tests for expected shortfall (ES) in the lower 10th percentile for U.S. 1-year and 10-year zero-coupon bond weekly log returns in different time windows. We report the change-point test statistics and the corresponding p-values. The top blocks show examples of where both the single and multiple change-point tests are significant. The middle blocks show examples of where the single change-point test is significant, but the multiple change-point test is not. The lower blocks show examples of where the multiple change-point test is significant, but the single change-point test is not.

1987 Black Monday Crash, the 2008 Global Financial Crisis, the 2011 August Market Decline, and the 2020 Covid-19 Pandemic. Similarly, for the 1-year and 10-year bond returns, the top block of Table 2 shows examples of time windows where both the single and multiple change-point tests detect change at the 0.05 significance level. In Figure 8, we plot the return time series for some of these time windows, including the 1980-1982 US recession (due in part to government restrictive

monetary policy, and to a lesser degree the Iranian Revolution of 1979, which resulted in significant oil price increases) and the 2008 Financial Crisis. These findings suggest that structural breaks in ES for stock returns closely align with major financial crises. This highlights the sensitivity of tail risk to systemic market disruptions. For bond returns, the detected breaks often coincide with significant shifts in monetary policy, which implies that changes in risk may reflect expectations about interest rate and policy uncertainty.

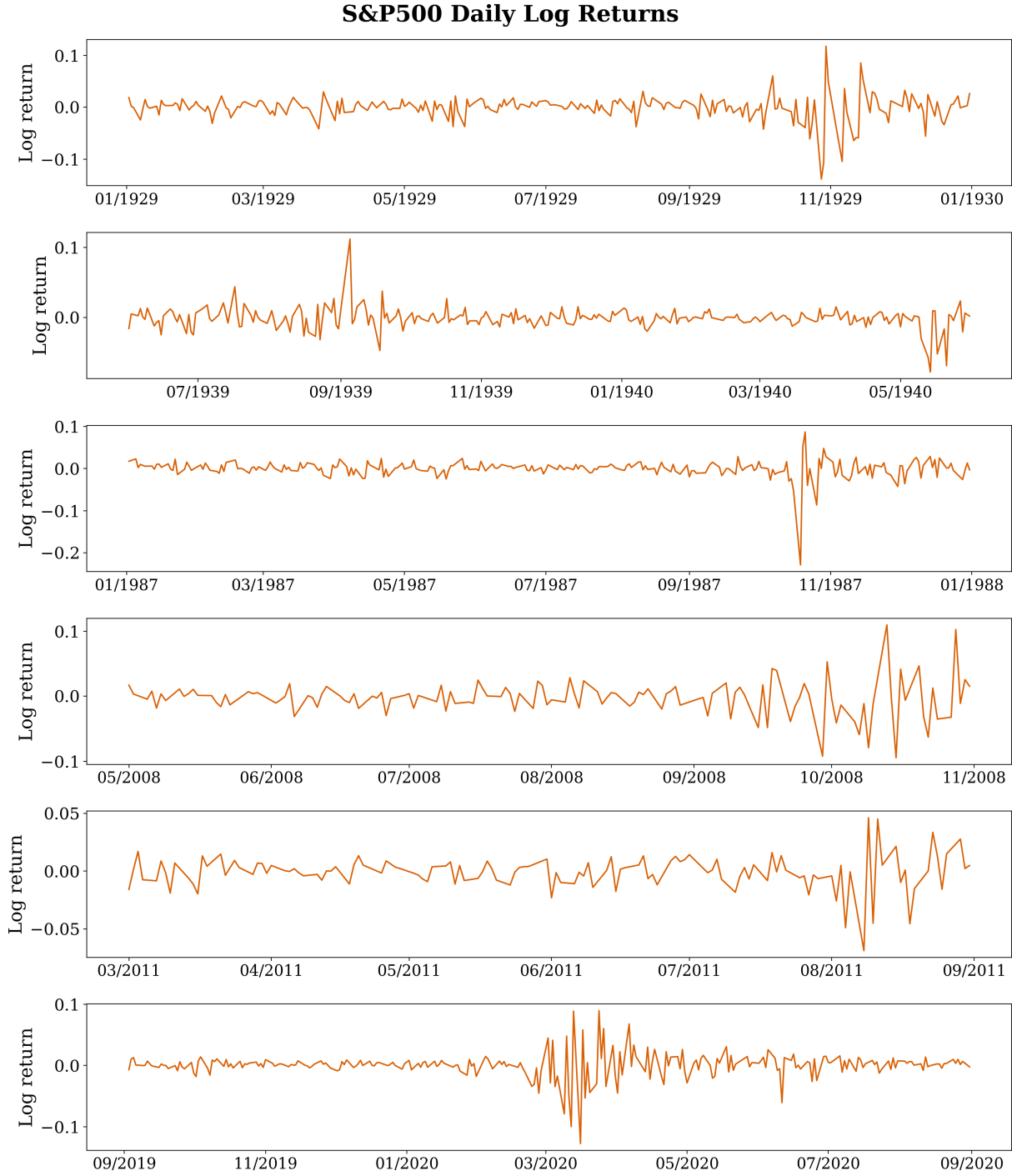
Interestingly, the change points detected for U.S. 1-year bond returns can differ from those for the U.S. 10-year bond returns. For example, during the period from August 05, 2012 to July 23, 2017, the p-values of both single and multiple-change tests for U.S. 1-year bond returns are less than 0.001, indicating the presence of change points. This is illustrated in the third plot in Figure 8. However, the p-values of both tests for U.S. 10-year bond returns exceed 0.7, suggesting no significant change points during the same period. This discrepancy might be due to the Federal Reserve's decision in 2015 to raise the federal funds rate, initiating a monetary tightening cycle after the Great Recession. Short-term yields, such as those on 1-year bonds, are directly tied to the federal funds rate and quickly reflect such policy changes. In contrast, long-term yields, such as those on 10-year bonds, are less sensitive to short-term policy changes and more influenced by long-term expectations of future economic growth and inflation.

On the other hand, different window sizes and change-point testing methods can yield different results. There are time windows where the single change-point test fails, but the multiple change-point test succeeds; see the bottom block of Table 1 for the S&P 500 daily returns. One example is the period between May 01, 2008 and April 30, 2009. Here, the p-value is 0.018 for the unsupervised multiple change-point test, with the test statistic (in (17)) having value 171.7, which indicates that there are one or more change points during this time window. However, the single change-point test performs poorly on this time window, with a p-value of 0.487 and the test statistic (in (15)) having a value of 8.0. As seen in Figure 7, changes in the tail of the distribution of the S&P 500 log returns are clearly present at the end of 2008, corresponding to the 2008 Financial Crisis. Because the single change-point test assumes that only one change point occurs and seeks to divide the time series into two sections separated by a single change point, the effects of multiple changes can be “canceled out”. The same issue arises for the U.S. 1-year bond log returns in the period from September 19, 1976 to August 31, 1986, and for U.S. 10-year bond log returns in the period from December 18, 1977 to November 29, 1987. This problem is addressed by the multiple change-point test.

However, there is also a trade-off associated with using the multiple change-point test, as it can suffer from low power when there is a single change point and the time window is short. This is supported by the examples in the middle block in Table 1 for the S&P 500 log returns. In these instances, the single change-point test has p-values that are all less than 0.025, but the multiple change-point test has p-values that are between 0.059 and 0.156. This suggests that the multiple change-point test detects some evidence of a change point, but not enough to achieve statistical significance at the 0.05 level.

In light of the above discussion, we recommend the following use of single and multiple change-point tests. In general, the multiple change-point test can be run first. If the test fails to reach

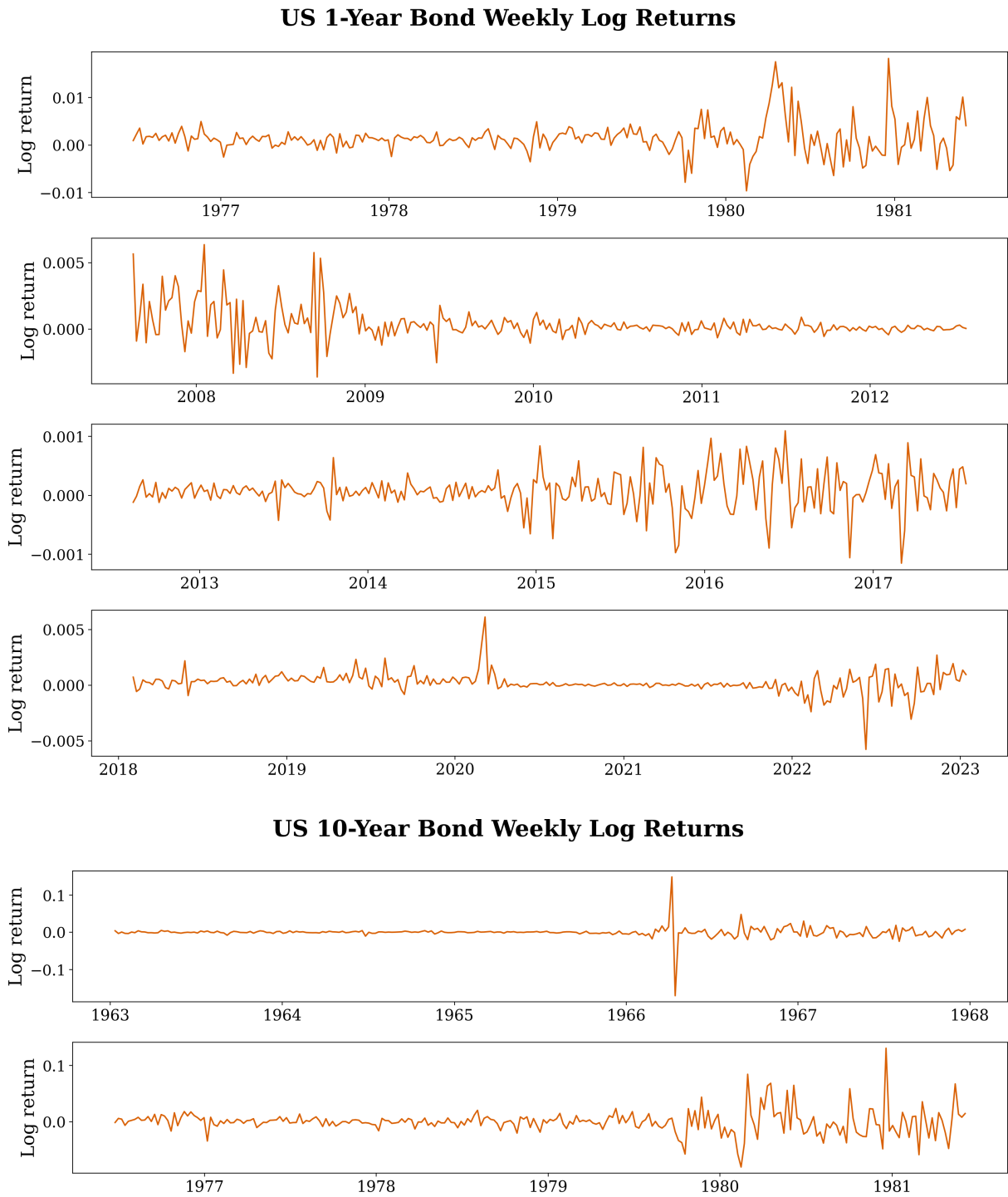
Figure 7: Examples of S&P 500 Return Time-Series Around Detected Change Points



This figure shows the S&P 500 log return time-series on local windows around suspected change points.

statistical significance, and it is plausible that there is only one change point, then to increase power, the single change-point test can be run (perhaps within a local window). Alternatively, the multiple change-point test can be used to check the result of the single change-point test, and help rule out the possibility that the effects of multiple changes are canceled out. In summary, the single

Figure 8: Examples of Bond Return Time-Series Around Detected Change Points



This figure shows the U.S. 1-year and 10-year bond log return time-series on local windows around suspected change points.

and multiple change-point tests can be deployed in complementary ways.

6 Conclusion

We propose a novel methodology to perform confidence interval construction and change-point testing for fundamental nonparametric estimators of risk such as ES. This allows for evaluation of the homogeneity of ES and related measures such as the conditional tail moments, and in particular allows the researcher to detect general tail structural changes in time series observations. While current approaches to tail structural change testing typically involve quantities such as the tail index and thus require parametric modeling of the tail, our approach does not require such assumptions. Moreover, we are able to detect more general structural changes in the tail using ES, for example, location and scale changes, which are undetectable using tail index. Hence, we advocate for the use of ES for general purpose monitoring for tail structural change.

We view our methods as being more robust compared to extant approaches which involve consistent estimation of standard errors or blockwise versions of the bootstrap or empirical likelihood, which can be more sensitive to tuning parameters. We note that our proposed sectioning and self-normalization methods for confidence interval construction and change-point testing still require some user choice, for example, the number of sections to use in sectioning or which particular functional to use for self-normalization. Our simulations demonstrate that our methods are robust to these user choices.

Our simulations show the promising finite-sample performance of our procedures. Our empirical study of S&P 500 and US Treasury bond returns illustrates the practical use of our methods in detecting and quantifying market instability via the tails of financial time series.

References

- T.W. Anderson. *The Statistical Analysis of Time Series*. Wiley, 1971.
- S. Asmussen and P.W. Glynn. *Stochastic Simulation: Algorithms and Analysis*. Springer-Verlag New York, 2007.
- Y. Benjamini and D. Yekutieli. The control of the false discovery rate in multiple testing under dependency. *The Annals of Statistics*, 29(4):1165–1188, 2001.
- P. Billingsley. *Convergence of Probability Measures*. Wiley, 1999.
- T. Bollerslev. Generalized autoregressive conditional heteroskedasticity. *Journal of Econometrics*, 31(3):307–327, 1986.
- P.J. Brockwell and R.A. Davis. *Time Series: Theory and Methods*. Springer-Verlag New York, 1991.
- A. Bucher. A note on weak convergence of the sequential multivariate empirical process under strong mixing. *Journal of Theoretical Probability*, 28(3):1028–1037, 2015.
- P. Bühlmann. Bootstraps for time series. *Statistical Science*, pages 52–72, 2002.

- S.X. Chen. Nonparametric estimation of expected shortfall. *Journal of Financial Econometrics*, 6(1):87–107, 2008.
- S.X. Chen and C.Y. Tang. Nonparametric inference of value-at-risk for dependent financial returns. *Journal of Financial Econometrics*, 3(2):227–255, 2005.
- C.M. Crainiceanu and T.J. Vogelsang. Nonmonotonic power for tests of a mean shift in a time series. *Journal of Statistical Computation and Simulation*, 77(6):457–476, 2007.
- M. Csorgo and L. Horvath. *Limit Theorems in Change-Point Analysis*. Wiley London, 1997.
- A. Deng and P. Perron. A non-local perspective on the power properties of the cusum and cusum of squares tests for structural change. *Journal of Econometrics*, 142(1):212–240, 2008.
- P. Doukhan. *Mixing, Properties and Examples, Lecture Notes in Statistics 85*. Springer-Verlag New York, 1994.
- P. Doukhan, P. Massart, and E. Rio. The functional central limit theorem for strongly mixing processes. *Ann. Inst. H. Poincaré Probab. Statist.*, 30(1):63–82, 1994.
- D. Filipovic, M. Pelger, and Y. Ye. Shrinking the term structure. *Working paper*, 2022.
- P.W. Glynn and D.L. Iglehart. Simulation output analysis using standardized time series. *Mathematics of Operations Research*, 15(1):1–16, 1990.
- B.M. Hill. A simple general approach to inference about the tail of a distribution. *The Annals of Statistics*, 3(5):1163–1174, 1975.
- Y. Hoga. Change point test for tail index for dependent data. *Econometric Theory*, 33(4):915–954, 2017.
- Lajos Horváth, Emese Lazar, Zhenya Liu, Shixuan Wang, and Xiaohan Xue. Sequential monitoring for changes in dynamic semiparametric risk models. *Available at SSRN 4722996*, 2024.
- M. Kim and S. Lee. Test for tail index change in stationary time series with Pareto-type marginal distribution. *Bernoulli*, 15(23):325–356, 2009.
- M. Kim and S. Lee. Change point test for tail index for dependent data. *Metrika*, 74(3):297–311, 2011.
- H.R. Kunsch. The jackknife and the bootstrap for general stationary observations. *The Annals of Statistics*, 17(3):1217–1241, 1989.
- R.Y. Liu and K. Singh. Efficiency and robustness in resampling. *The Annals of Statistics*, 20(1):370–384, 1992.
- I.N. Lobato. Testing that a dependent process is uncorrelated. *Journal of the American Statistical Association*, 96(455):1066–1076, 2001.

- A.J. McNeil, R. Frey, and P. Embrechts. *Quantitative Risk Management: Concepts, Techniques and Tools - Revised Edition*. Princeton University Press, 2015.
- J.E. Methni, L. Gardes, and S. Girard. Non-parametric estimation of extreme risk measures from conditional heavy-tailed distributions. *Scandinavian Journal of Statistics*, 41(4):988–1012, 2014.
- E.S. Page. Continuous inspection schemes. *Biometrika*, 41(1/2):100–115, 1954.
- D.N. Politis, J.P. Romano, and M. Wolf. *Subsampling*. Springer-Verlag New York, 1999.
- Z. Qu. Testing for structural change in regression quantiles. *Journal of Econometrics*, 146(1):170–184, 2008.
- M. Rocco. Extreme value theory in finance: A survey. *Journal of Economic Surveys*, 28(1):82–108, 2014.
- M. Rosenblatt. Remarks on some nonparametric estimates of a density function. *The Annals of Mathematical Statistics*, 27(3):832–837, 1956.
- L. Schruben. Confidence interval estimation using standardized time series. *Operations Research*, 31(6):1090–1108, 1983.
- P.K. Sen. On the Bahadur representation of sample quantiles for sequences of φ -mixing random variables. *Journal of Multivariate Analysis*, 2(1):77–95, 1972.
- Q.M. Shao and H. Yu. Weak convergence for weighted empirical processes of dependent sequences. *The Annals of Probability*, 24(4):2098–2127, 1996.
- X. Shao. A self-normalized approach to confidence interval construction in time series. *Journal of the Royal Statistical Society B*, 72(3):343–366, 2010.
- X. Shao and X. Zhang. Testing for change points in time series. *Journal of the American Statistical Association*, 105(491):1228–1240, 2010.
- L. Sun and J.L. Hong. Asymptotic representations for importance-sampling estimators of value-at-risk and conditional value-at-risk. *Operations Research Letters*, 38(4):246–251, 2010.
- A.W. van der Vaart. *Asymptotic Statistics*. Cambridge University Press, 1998.
- A.W. van der Vaart and J.A. Wellner. *Weak Convergence and Empirical Processes*. Springer-Verlag New York, 1996.
- T.J. Vogelsang. Sources of nonmonotonic power when testing for a shift in mean of a dynamic time series. *Journal of Econometrics*, 88(2):283–299, 1999.
- C.S. Wang and Z. Zhao. Conditional value-at-risk: Semiparametric estimation and inference. *Journal of Econometrics*, 195(1):86–103, 2016.
- M. Wendler. Bahadur representation for U-quantiles of dependent data. *Journal of Multivariate Analysis*, 102(6):1064–1079, 2011.

G.D. Xing, S.C. Yang, Y. Liu, and K.M. Yu. A note on the Bahadur representation of sample quantiles for α -mixing random variables. *Monatshefte für Mathematik*, 165(3):579–596, 2012.

K.L. Xu. Model-free inference for tail risk measures. *Econometric Theory*, 32(1):122–153, 2016.

T. Zhang and L. Lavitas. Unsupervised self-normalized change-point testing for time series. *Journal of the American Statistical Association*, 0(0):1–12, 2018.

Appendix

Appendix A: Proofs

In what follows, let $p \in (0, 1)$ be a fixed probability level of interest for VaR, ES and their estimators. To keep notation simple in our proofs, we use the shorthand $q := \text{VaR}(p)$, and based on samples X_1, \dots, X_n , we set $\widehat{Q}_n := \widehat{\text{VaR}}_n$ and $\widehat{F}_n(\cdot)$ denote the empirical distribution function. We let $\widehat{Q}_{l:m}$ denote the VaR estimator and $\widehat{F}_{l:m}(\cdot)$ the empirical distribution function based on samples X_l, \dots, X_m . For a sample X_1, X_2, \dots, X_n , denote the order statistics by $X_{n,1} \leq X_{n,2} \leq \dots \leq X_{n,n}$.

Proof of Theorem 1

First, for VaR, we show that

$$\sup_{t \in [0,1]} \sqrt{nt} \left| \widehat{Q}_{[nt]} - q - f(q)^{-1}(\widehat{F}_{[nt]}(q) - p) \right| = o_P(1). \quad (20)$$

As in the proof of Theorem 6.2 of Sen (1972), let $\epsilon > 0$, and for every positive integer k , define

$$k^* = |q(k^{-1-\epsilon})| + |q(1-k^{-1-\epsilon})| + 1.$$

Consider a sequence k_n of positive integers such that $k_n \rightarrow \infty$, but $n^{-1/2}k_n k_n^* \rightarrow 0$. We then have

$$\begin{aligned} & \sup_{t \in [0,1]} \sqrt{nt} \left| \widehat{Q}_{[nt]} - q - f(q)^{-1}(\widehat{F}_{[nt]}(q) - p) \right| \\ & \leq \sup_{t \in [0, n^{-1}k_n]} \sqrt{nt} \left| \widehat{Q}_{[nt]} - q \right| + \sup_{t \in [0, n^{-1}k_n]} \sqrt{nt} \left| f(q)^{-1}(\widehat{F}_{[nt]}(q) - p) \right| \\ & \quad + \sup_{t \in [n^{-1}k_n, 1]} \sqrt{nt} \left| \widehat{Q}_{[nt]} - q - f(q)^{-1}(\widehat{F}_{[nt]}(q) - p) \right|. \end{aligned}$$

For the first term on the right hand side, notice that

$$\sup_{t \in [0, n^{-1}k_n]} \sqrt{nt} \left| \widehat{Q}_{[nt]} - q \right| = \max_{1 \leq k \leq k_n} \frac{k}{\sqrt{n}\sigma} \left| \widehat{Q}_k - q \right| \leq \frac{k_n}{\sqrt{n}\sigma} (|X_{k_n, k_n} - q| + |X_{k_n, 1} - q|).$$

Then, with $n(1 - F(X_{n,n}))$ converging in distribution to a standard exponential,

$$\mathbb{P}(q \leq X_{k_n, k_n} \leq q(1 - k_n^{-1-\epsilon})) = \mathbb{P}(k_n(1 - p) \geq k_n(1 - F(X_{k_n, k_n})) \geq k_n^{-\epsilon}) \rightarrow 1.$$

Similarly, with $nF(X_{n,1})$ converging in distribution to a standard exponential,

$$\mathbb{P}(q(k_n^{-1-\epsilon}) \leq X_{k_n,1} \leq q) = \mathbb{P}(k_n^{-\epsilon} \leq k_n F(X_{k_n,1}) \leq k_n p) \rightarrow 1.$$

So asymptotically with probability one,

$$|q(1 - k_n^{-1-\epsilon}) - q| \geq |X_{k_n,k_n} - q|$$

$$|q(k_n^{-1-\epsilon}) - q| \geq |X_{k_n,1} - q|.$$

Thus, asymptotically with probability one,

$$\sup_{t \in [0, n^{-1}k_n]} \sqrt{nt} |\widehat{Q}_{[nt]} - q| \leq \frac{k_n}{\sqrt{n}\sigma} (k_n^* + 2|q|) \rightarrow 0.$$

Under Assumption 1 and the functional convergence $\sqrt{nt}f(q)^{-1}(\widehat{F}_{[nt]}(q) - p) \xrightarrow{d} \sigma W(t)$ for some $\sigma \geq 0$ (see, for example, Theorem 1 of Doukhan et al. (1994)), we have

$$\sup_{t \in [0, n^{-1}k_n]} \sqrt{nt} |f(q)^{-1}(\widehat{F}_{[nt]}(q) - p)| \xrightarrow{P} 0.$$

Lastly, by the Bahadur representation for \widehat{Q}_n in Theorem 1 of Wendler (2011), which holds under Assumption 1,

$$\begin{aligned} & \sup_{t \in [n^{-1}k_n, 1]} \sqrt{nt} |\widehat{Q}_{[nt]} - q - f(q)^{-1}(\widehat{F}_{[nt]}(q) - p)| \\ &= \max_{k_n \leq k \leq n} \frac{1}{\sqrt{n}} k |\widehat{Q}_k - q - f(q)^{-1}(\widehat{F}_k(q) - p)| \\ &= \max_{k_n \leq k \leq n} \frac{1}{\sqrt{n}} k o_{a.s.}(k^{-5/8}(\log k)^{3/4}(\log \log k)^{1/2}) \\ &= o_{a.s.}(1), \end{aligned}$$

and we have established (20).

Next, for ES, we show that

$$\sup_{t \in [0, 1]} \frac{1}{\sqrt{n}} \left| \frac{1}{1-p} \sum_{k=1}^{[nt]} X_k \mathbb{I}(\widehat{Q}_{[nt]} \leq X_k) - \left([nt]q + \frac{1}{1-p} \sum_{k=1}^{[nt]} [X_k - q]_+ \right) \right| = o_P(1). \quad (21)$$

Using (28) from the proof of Proposition 1, we have

$$\begin{aligned}
& \sup_{t \in [0,1]} \frac{1}{\sqrt{n}} \left| \frac{1}{1-p} \sum_{k=1}^{[nt]} X_k \mathbb{I}(\widehat{Q}_{[nt]} \leq X_k) - \left([nt]q + \frac{1}{1-p} \sum_{k=1}^{[nt]} [X_k - q]_+ \right) \right| \\
& \leq \sup_{t \in [0,1]} \frac{1}{1-p} \frac{[nt]}{\sqrt{n}} \left(|q| |\widehat{F}_{[nt]}(\widehat{Q}_{[nt]}) - p| + |\widehat{Q}_{[nt]} - q| (3 |\widehat{F}_{[nt]}(\widehat{Q}_{[nt]}) - p| + |\widehat{F}_{[nt]}(q) - p|) \right) \\
& = \sup_{1 \leq k \leq n} \frac{1}{1-p} \frac{k}{\sqrt{n}} \left(|q| |\widehat{F}_k(\widehat{Q}_k) - p| + |\widehat{Q}_k - q| (3 |\widehat{F}_k(\widehat{Q}_k) - p| + |\widehat{F}_k(q) - p|) \right).
\end{aligned}$$

Observe that for some $C > 0$, we have

$$\sup_{1 \leq k \leq n} \frac{1}{1-p} \frac{k}{\sqrt{n}} |q| |\widehat{F}_k(\widehat{Q}_k) - p| \stackrel{a.s.}{\leq} C \frac{1}{1-p} \frac{1}{\sqrt{n}} |q| = O(n^{-1/2}).$$

Let $k_n \rightarrow \infty$ be the sequence as used above in the proof of (20) for VaR. Then observe that

$$\begin{aligned}
& \sup_{1 \leq k \leq n} \frac{1}{1-p} \frac{k}{\sqrt{n}} |\widehat{Q}_k - q| (3 |\widehat{F}_k(\widehat{Q}_k) - p| + |\widehat{F}_k(q) - p|) \\
& \leq \sup_{1 \leq k \leq k_n} \frac{4}{1-p} \frac{k}{\sqrt{n}} |\widehat{Q}_k - q| + \sup_{k_n \leq k \leq n} \frac{1}{1-p} \frac{k}{\sqrt{n}} |\widehat{Q}_k - q| (3 |\widehat{F}_k(\widehat{Q}_k) - p| + |\widehat{F}_k(q) - p|).
\end{aligned}$$

As was shown in the proof of (20) for VaR,

$$\sup_{1 \leq k \leq k_n} \frac{4}{1-p} \frac{k}{\sqrt{n}} |\widehat{Q}_k - q| = o_{a.s.}(1).$$

Finally, using the Bahadur representation from Proposition 1, we have

$$\begin{aligned}
& \sup_{k_n \leq k \leq n} \frac{1}{1-p} \frac{k}{\sqrt{n}} |\widehat{Q}_k - q| (3 |\widehat{F}_k(\widehat{Q}_k) - p| + |\widehat{F}_k(q) - p|) \\
& \leq \sup_{k_n \leq k \leq n} \frac{1}{1-p} \frac{k}{\sqrt{n}} o_{a.s.}(k^{-1+1/(2a)+\gamma'} \log k) \\
& \leq \sup_{k_n \leq k \leq n} \frac{1}{1-p} o_{a.s.}(k^{-1/2+1/(2a)+\gamma'} \log k) \\
& = o_{a.s.}(1).
\end{aligned}$$

The last equality is due to $-1/2 + 1/(2a) + \gamma' < 0$, as in the proof of Proposition 1. We have thus shown the stronger version of (21):

$$\sup_{t \in [0,1]} \frac{1}{\sqrt{n}} \left| \frac{1}{1-p} \sum_{k=1}^{[nt]} X_k \mathbb{I}(\widehat{Q}_{[nt]} \leq X_k) - \left([nt]q + \frac{1}{1-p} \sum_{k=1}^{[nt]} [X_k - q]_+ \right) \right| = o_{a.s.}(1). \quad (22)$$

By Theorem 1 of Doukhan et al. (1994) (and the remark following the theorem), under As-

sumption 1, the bivariate process

$$\left\{ \frac{1}{\sqrt{n}} \sum_{k=1}^{[nt]} \begin{bmatrix} f(q)^{-1}(\mathbb{I}(X_k \leq q) - p) \\ (1-p)^{-1}([X_k - q]_+ - \mathbb{E}[[X_k - q]_+]) \end{bmatrix} : t \in [0, 1] \right\} \quad (23)$$

converges in distribution in $D[0, 1] \times D[0, 1]$ to $\Sigma(W_1, W_2)$, where W_1 and W_2 are independent standard Brownian motions and $\Sigma \in \mathbb{R}^{2 \times 2}$ is a positive semidefinite matrix with components (6)-(8). In light of (20) and (21), the proof is complete.

Proof of Proposition 1

First, we have

$$\begin{aligned} & \left| \frac{1}{1-p} \frac{1}{n} \sum_{k=1}^n X_k \mathbb{I}(\hat{Q}_n \leq X_k) - \left(\hat{Q}_n + \frac{1}{1-p} \frac{1}{n} \sum_{k=1}^n [X_k - \hat{Q}_n]_+ \right) \right| \\ & \leq \frac{1}{1-p} |\hat{Q}_n| |\hat{F}_n(\hat{Q}_n) - p|. \end{aligned} \quad (24)$$

Next, observe the following.

$$\begin{aligned} & \left| \left(\hat{Q}_n + \frac{1}{1-p} \frac{1}{n} \sum_{k=1}^n [X_k - \hat{Q}_n]_+ \right) - \left(q + \frac{1}{1-p} \frac{1}{n} \sum_{k=1}^n [X_k - q]_+ \right) \right| \\ & = \left| (\hat{Q}_n - q) + \frac{1}{1-p} \frac{1}{n} \sum_{k=1}^n (q - \hat{Q}_n) \mathbb{I}(\hat{Q}_n \leq X_k) + \frac{1}{1-p} \frac{1}{n} \sum_{k=1}^n (X_k - q) (\mathbb{I}(\hat{Q}_n \leq X_k) - \mathbb{I}(q \leq X_k)) \right| \\ & \stackrel{a.s.}{=} \left| \frac{1}{1-p} (\hat{Q}_n - q) (\hat{F}_n(\hat{Q}_n) - p) + \frac{1}{1-p} \frac{1}{n} \sum_{k=1}^n (X_k - q) (\mathbb{I}(\hat{Q}_n \leq X_k) - \mathbb{I}(q \leq X_k)) \right| \\ & \leq \frac{1}{1-p} |\hat{Q}_n - q| |\hat{F}_n(\hat{Q}_n) - p| + \left| \frac{1}{1-p} \frac{1}{n} \sum_{k=1}^n (X_k - q) (\mathbb{I}(\hat{Q}_n \leq X_k) - \mathbb{I}(q \leq X_k)) \right| \\ & \leq \frac{1}{1-p} |\hat{Q}_n - q| |\hat{F}_n(\hat{Q}_n) - p| + \frac{1}{1-p} |\hat{Q}_n - q| \left| \frac{1}{n} \sum_{k=1}^n \mathbb{I}(\hat{Q}_n \leq X_k) - \frac{1}{n} \sum_{k=1}^n \mathbb{I}(q \leq X_k) \right| \\ & \stackrel{a.s.}{=} \frac{1}{1-p} |\hat{Q}_n - q| |\hat{F}_n(\hat{Q}_n) - p| + \frac{1}{1-p} |\hat{Q}_n - q| |\hat{F}_n(\hat{Q}_n) - \hat{F}_n(q)| \\ & \leq \frac{1}{1-p} |\hat{Q}_n - q| (2 |\hat{F}_n(\hat{Q}_n) - p| + |\hat{F}_n(q) - p|) \end{aligned} \quad (25)$$

Under the assumptions of Proposition 1, $\left| \widehat{F}_n(\widehat{Q}_n) - p \right| = O_{a.s.}(n^{-1})$, which can be seen via the following arguments. Let \mathcal{O} denote the neighborhood of q in Assumption 1 (iii).

$$\begin{aligned} \left| \widehat{F}_n(\widehat{Q}_n) - p \right| &\leq n^{-1} \sum_{k=1}^n \mathbb{I}(\widehat{Q}_n = X_k) \\ &\leq n^{-1} + \mathbb{I}(\widehat{Q}_n = X_i = X_j, i \neq j) \\ &= n^{-1} + \mathbb{I}(\widehat{Q}_n = X_i = X_j, i \neq j, \widehat{Q}_n \in \mathcal{O}) + \mathbb{I}(\widehat{Q}_n = X_i = X_j, i \neq j, \widehat{Q}_n \notin \mathcal{O}) \\ &\leq n^{-1} + \mathbb{I}(X_i = X_j, i \neq j, X_i \in \mathcal{O}) + \mathbb{I}(\widehat{Q}_n \notin \mathcal{O}) \\ &\stackrel{a.s.}{=} n^{-1} + \mathbb{I}(\widehat{Q}_n \notin \mathcal{O}) \end{aligned} \quad (26)$$

$$\stackrel{a.s.}{=} n^{-1} \quad (27)$$

In the above, (26) is due to Assumption 1 (iii), and (27) holds for sufficiently large n due to strong consistency of \widehat{Q}_n under the assumptions of Proposition 1, as established in Theorem 2.1 of Xing et al. (2012). Also, by Theorem 2.1 of Xing et al. (2012), $\left| \widehat{Q}_n - q \right| = o_{a.s.}(n^{-1/2} \log n)$.

Now we examine the term $\left| \widehat{F}_n(q) - p \right|$. Let $\gamma' > 0$ such that $-1/2 + 1/(2a) + \gamma' < 0$. Note that

$$\begin{aligned} \mathbb{P}\left(\left| \widehat{F}_n(q) - p \right| > n^{-1/2+1/(2a)+\gamma'}\right) &= \mathbb{P}\left(\left| \sum_{k=1}^n (\mathbb{I}(X_k \leq q) - p) \right| > n^{1/2+1/(2a)+\gamma'}\right) \\ &\leq \frac{\mathbb{E}\left[\left| \sum_{k=1}^n (\mathbb{I}(X_k \leq q) - p) \right|^{2a}\right]}{n^{a+1+2a\gamma'}} \\ &\leq \frac{Kn^a}{n^{a+1+2a\gamma'}} \\ &= Kn^{-1-2a\gamma'}. \end{aligned}$$

The second inequality above is due to Theorem 4.1 of Shao and Yu (1996), where K is a global constant depending only on $C > 0$ and $a > 1$ ensuring that $\alpha(n) \leq Cn^{-a}$ for all n . Since $\sum_{n=1}^{\infty} Kn^{-1-2a\gamma'} < \infty$, the Borel-Cantelli Lemma yields:

$$\left| \widehat{F}_n(q) - p \right| = O_{a.s.}(n^{-1/2+1/(2a)+\gamma'}).$$

Finally, putting together (24) and (25) yields the following.

$$\begin{aligned}
& \left| \frac{1}{1-p} \frac{1}{n} \sum_{k=1}^n X_k \mathbb{I}(\hat{Q}_n \leq X_k) - \left(q + \frac{1}{1-p} \frac{1}{n} \sum_{k=1}^n [X_k - q]_+ \right) \right| \\
& \leq \frac{1}{1-p} \left(|\hat{Q}_n| |\hat{F}_n(\hat{Q}_n) - p| + |\hat{Q}_n - q| (2 |\hat{F}_n(\hat{Q}_n) - p| + |\hat{F}_n(q) - p|) \right) \\
& \leq \frac{1}{1-p} \left(|q| |\hat{F}_n(\hat{Q}_n) - p| + |\hat{Q}_n - q| |\hat{F}_n(\hat{Q}_n) - p| + |\hat{Q}_n - q| (2 |\hat{F}_n(\hat{Q}_n) - p| + |\hat{F}_n(q) - p|) \right) \\
& = \frac{1}{1-p} \left(|q| |\hat{F}_n(\hat{Q}_n) - p| + |\hat{Q}_n - q| (3 |\hat{F}_n(\hat{Q}_n) - p| + |\hat{F}_n(q) - p|) \right) \\
& = o_{a.s.}(n^{-1+1/(2a)+\gamma'} \log n)
\end{aligned} \tag{28}$$

Proof of Theorem 2

Recall the definition of the index set $\Delta = \{s, t \in [0, 1], t - s \geq \delta\}$, with $\delta > 0$. First, for VaR, we show that

$$\sup_{(s,t) \in \Delta} \sqrt{n} \left| \hat{Q}_{[ns]+1:[nt]} - q - f(q)^{-1}(\hat{F}_{[ns]+1:[nt]}(q) - p) \right| = o_P(1). \tag{29}$$

By Theorem 1 of Bucher (2015), the sequential empirical process

$$\left\{ \frac{1}{\sqrt{n}} \sum_{i=1}^{[nt]} (\mathbb{I}(X_i \leq x) - F(x)) : (t, x) \in [0, 1] \times \mathbb{R} \right\}$$

converges in distribution in $\ell^\infty([0, 1] \times \mathbb{R})$ to a Gaussian process $\{Y(t, x) : (t, x) \in [0, 1] \times \mathbb{R}\}$. Consider the mapping from $\ell^\infty([0, 1] \times \mathbb{R}) \rightarrow \ell^\infty(\Delta \times \mathbb{R})$ given by $\{Y(t, x) : (t, x) \in [0, 1] \times \mathbb{R}\} \mapsto \{Y(t, x) - Y(s, x) : (s, t, x) \in \Delta \times \mathbb{R}\}$. This is a continuous mapping when both spaces are endowed with their uniform topologies. Then, the Continuous Mapping Theorem yields convergence in distribution of the process

$$\left\{ \frac{1}{\sqrt{n}} \sum_{k=[ns]+1}^{[nt]} (\mathbb{I}(X_i \leq x) - F(x)) : ((s, t), x) \in \Delta \times \mathbb{R} \right\}$$

in $\ell^\infty(\Delta \times \mathbb{R})$ to a Gaussian process $\{Z(s, t, x) : (s, t, x) \in \Delta \times \mathbb{R}\}$. As discussed in Example 3.9.21 of van der Vaart and Wellner (1996), for fixed $p \in (0, 1)$, the mapping from a distribution function to its VaR at level p : $F \mapsto F^{-1}(p)$ is Hadamard-differentiable at every distribution function F that is differentiable at $F^{-1}(p)$ with strictly positive derivative $f(F^{-1}(p))$, tangentially to the set of functions that are continuous at $F^{-1}(p)$. By the Functional Delta Method (see, for example, Theorem 3.9.4 of van der Vaart and Wellner (1996)), (29) is established.

Next, for ES, we show that

$$\sup_{(s,t) \in \Delta} \frac{1}{\sqrt{n}} \left| \frac{1}{1-p} \sum_{k=[ns]+1}^{[nt]} X_k \mathbb{I}(X_k \geq \widehat{Q}_{[ns]+1:[nt]}) - \left(([nt]-[ns])q + \frac{1}{1-p} \sum_{k=[ns]+1}^{[nt]} [X_k - q]_+ \right) \right| = o_P(1). \quad (30)$$

Using (28) from the proof of Proposition 1, we have

$$\begin{aligned} & \sup_{(s,t) \in \Delta} \frac{1}{\sqrt{n}} \left| \frac{1}{1-p} \sum_{k=[ns]+1}^{[nt]} X_k \mathbb{I}(X_k \geq \widehat{Q}_{[ns]+1:[nt]}) - \left(([nt]-[ns])q + \frac{1}{1-p} \sum_{k=[ns]+1}^{[nt]} [X_k - q]_+ \right) \right| \\ & \leq \sup_{(s,t) \in \Delta} \frac{1}{1-p} \frac{[nt]-[ns]}{\sqrt{n}} \left(|q| |\widehat{F}_{[ns]+1:[nt]}(\widehat{Q}_{[ns]+1:[nt]}) - p| \right. \\ & \quad \left. + |\widehat{Q}_{[ns]+1:[nt]} - q| \left(3 |\widehat{F}_{[ns]+1:[nt]}(\widehat{Q}_{[ns]+1:[nt]}) - p| + |\widehat{F}_{[ns]+1:[nt]}(q) - p| \right) \right). \end{aligned}$$

By the assumption that (X_1, X_k) has joint density for all $k \geq 2$, there can be no ties among X_1, X_2, \dots . So with $\delta > 0$ from the definition of the index set Δ ,

$$\sup_{(s,t) \in \Delta} \left| \widehat{F}_{[ns]+1:[nt]}(\widehat{Q}_{[ns]+1:[nt]}) - p \right| \leq \frac{1}{[nt]-[ns]}.$$

Hence, it suffices to show, as $n \rightarrow \infty$,

$$\sup_{(s,t) \in \Delta} \frac{[nt]-[ns]}{\sqrt{n}} \left| \widehat{Q}_{[ns]+1:[nt]} - q \right| \left| \widehat{F}_{[ns]+1:[nt]}(q) - p \right| = o_P(1).$$

In light of our above arguments and the result for VaR established above, as $n \rightarrow \infty$,

$$\begin{aligned} & \sup_{(s,t) \in \Delta} \sqrt{n}(t-s) \left| \widehat{F}_{[ns]+1:[nt]}(q) - p \right| = O_P(1) \\ & \sup_{(s,t) \in \Delta} \sqrt{n}(t-s) \left| \widehat{Q}_{[ns]+1:[nt]} - q \right| = O_P(1), \end{aligned}$$

from which (30) follows.

Consider the mapping from $\ell^\infty([0, 1]) \rightarrow \ell^\infty(\Delta)$ given by $\{Y(t) : (t) \in [0, 1]\} \mapsto \{Y(t) - Y(s) : (s, t) \in \Delta\}$. By the Continuous Mapping Theorem and the convergence in distribution of the process in (23) (from the proof of Theorem 1), we have that

$$\left\{ \frac{1}{\sqrt{n}} \sum_{k=[ns]+1}^{[nt]} \left[\frac{f(q)^{-1}(\mathbb{I}(X_k \leq q) - p)}{(1-p)^{-1}([X_k - q]_+ - \mathbb{E}[[X_k - q]_+])} \right] : (s, t) \in \Delta \right\} \quad (31)$$

converges in distribution in $\ell^\infty(\Delta) \times \ell^\infty(\Delta)$ to the process in (10). In light of (29) and (30), the proof is complete.

Proof of Proposition 2

We are concerned with the following variant of the CUSUM process:

$$\left\{ \frac{1}{\sqrt{n}} \left(\frac{n - [nt]}{n} \sum_{k=1}^{[nt]} \frac{X_k \mathbb{I}(\widehat{Q}_{1:[nt]} \leq X_k)}{1-p} - \frac{[nt]}{n} \sum_{k=[nt]+1}^n \frac{X_k \mathbb{I}(\widehat{Q}_{[nt]+1:n} \leq X_k)}{1-p} \right) : t \in [0, 1] \right\}.$$

Under Assumption 1, using Theorem 1, it is straightforward to obtain convergence in distribution in $D[0, 1]$ of the above process to $\sigma' B$, where $B(t) := W(t) - tW(1)$ (for $t \in [0, 1]$) is a standard Brownian bridge on $[0, 1]$ and $\sigma' \geq 0$. Note that

$$\left\{ \frac{1}{\sqrt{n}} \left(\frac{n - [nt]}{n} \sum_{k=1}^{[nt]} \frac{\max(X_k, q)}{1-p} - \frac{[nt]}{n} \sum_{k=[nt]+1}^n \frac{\max(X_k, q)}{1-p} \right) : t \in [0, 1] \right\}$$

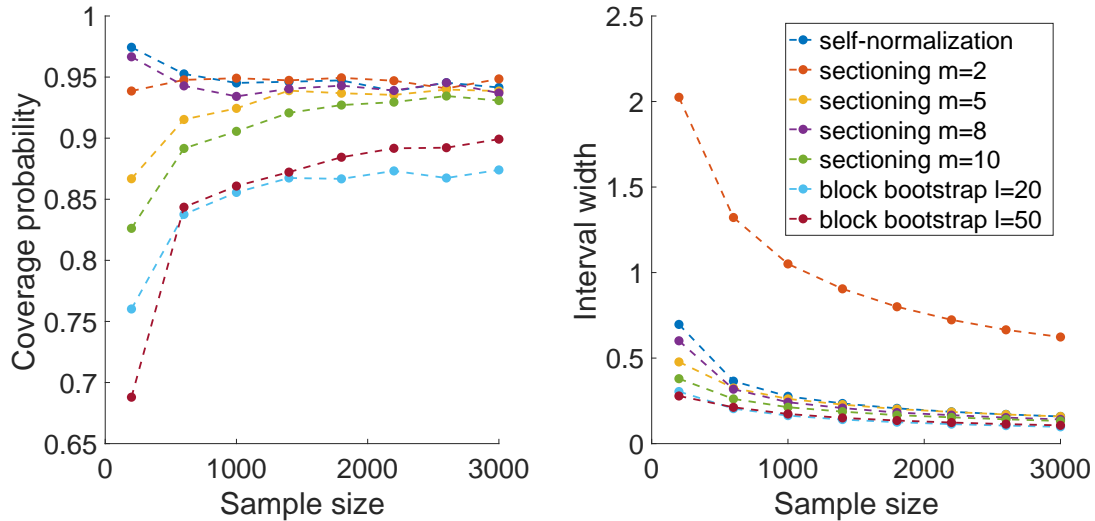
converges in distribution in $D[0, 1]$ to $\sigma' B$. Then, we get the desired conclusion by observing the following.

$$\begin{aligned} & \sup_{t \in [0, 1]} \frac{1}{\sqrt{n}} \left| \frac{n - [nt]}{n} \sum_{k=1}^{[nt]} \frac{X_k \mathbb{I}(\widehat{Q}_{1:[nt]} \leq X_k)}{1-p} - \frac{[nt]}{n} \sum_{k=[nt]+1}^n \frac{X_k \mathbb{I}(\widehat{Q}_{[nt]+1:n} \leq X_k)}{1-p} \right. \\ & \quad \left. - \frac{n - [nt]}{n} \sum_{k=1}^{[nt]} \frac{\max(X_k, q)}{1-p} + \frac{[nt]}{n} \sum_{k=[nt]+1}^n \frac{\max(X_k, q)}{1-p} \right| \\ & \leq \sup_{t \in [0, 1]} \frac{1}{\sqrt{n}} \left| \sum_{k=1}^{[nt]} \frac{X_k \mathbb{I}(\widehat{Q}_{1:[nt]} \leq X_k)}{1-p} - \sum_{k=1}^{[nt]} \frac{\max(X_k, q) - qp}{1-p} \right| \\ & \quad + \sup_{t \in [0, 1]} \frac{1}{\sqrt{n}} \left| \sum_{k=[nt]+1}^n \frac{X_k \mathbb{I}(\widehat{Q}_{[nt]+1:n} \leq X_k)}{1-p} - \sum_{k=[nt]+1}^n \frac{\max(X_k, q) - qp}{1-p} \right| \\ & \leq \sup_{t \in [0, 1]} \frac{1}{\sqrt{n}} \left| \sum_{k=1}^{[nt]} \frac{X_k \mathbb{I}(\widehat{Q}_{1:[nt]} \leq X_k)}{1-p} - \left([nt]q + \sum_{k=1}^{[nt]} \frac{[X_k - q]_+}{1-p} \right) \right| \\ & \quad + \sup_{t \in [0, 1]} \frac{1}{\sqrt{n}} \left| \sum_{k=[nt]+1}^n \frac{X_k \mathbb{I}(\widehat{Q}_{[nt]+1:n} \leq X_k)}{1-p} - \left((n - [nt])q + \sum_{k=[nt]+1}^n \frac{[X_k - q]_+}{1-p} \right) \right| \\ & = o_p(1) \end{aligned}$$

The convergence in probability to zero follows by stationarity of the sequence X_1, X_2, \dots and (22) from the proof of Theorem 1.

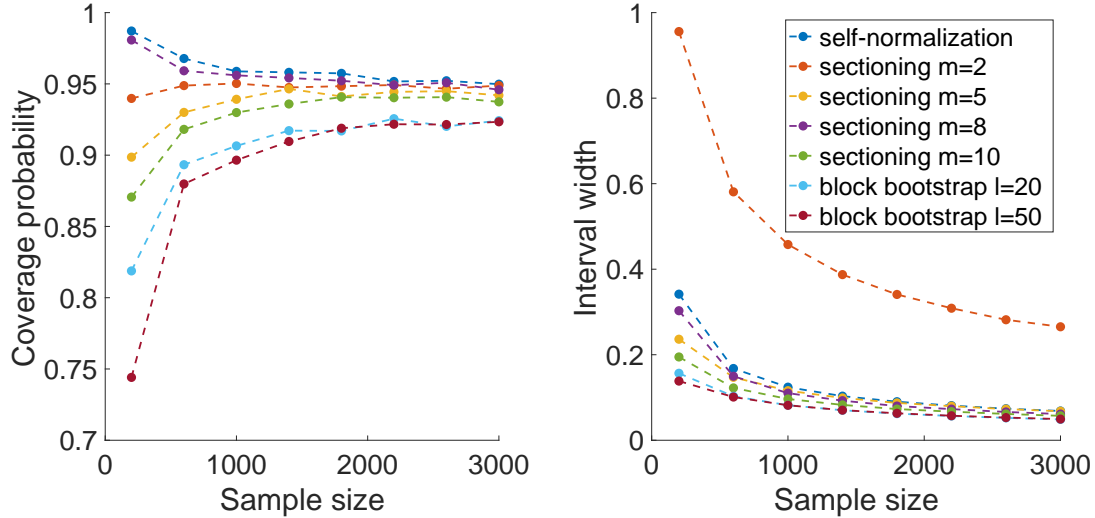
Appendix B: Simulations

Figure A.1: Coverage Probability and Confidence Intervals for GARCH(1,1) with i.i.d. Normal Innovations and Parameters $\lambda_1 = 0.05$ and $\lambda_2 = 0.9$



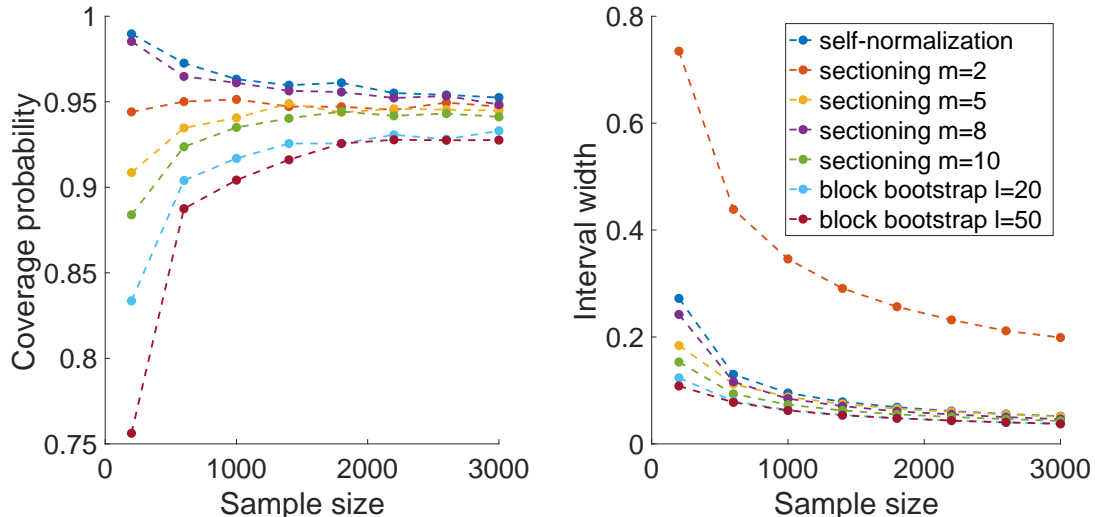
This figure shows the coverage probability and confidence interval width for different sample size. We use the GARCH(1,1) process with i.i.d. standard normal innovations, and set the model parameters as $\omega = 0.01$, $\lambda_1 = 0.05$, and $\lambda_2 = 0.9$. Left subfigure: relationship between sample size and empirical coverage probability of 95% confidence intervals for ES in the upper 5th percentile computed for stationary GARCH(1,1) process. Right subfigure: relationship between time series sample size and width of 95% confidence intervals for ES in the upper 5th percentile computed for stationary GARCH(1,1) process. Each plotted point is the averaged result over 10,000 replications.

Figure A.2: Coverage Probability and Confidence Intervals for GARCH(1,1) with i.i.d. Normal Innovations and Parameters $\lambda_1 = 0.1$ and $\lambda_2 = 0.7$



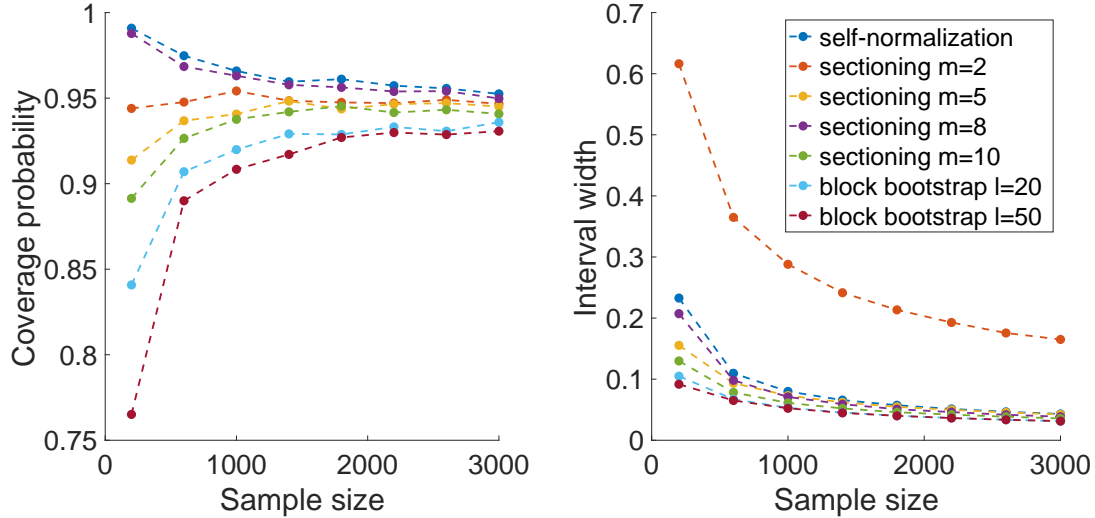
This figure shows the coverage probability and confidence interval width for different sample size. We use the GARCH(1,1) process with i.i.d. standard normal innovations, and set the model parameters as $\omega = 0.01$, $\lambda_1 = 0.1$, and $\lambda_2 = 0.7$. Left subfigure: relationship between sample size and empirical coverage probability of 95% confidence intervals for ES in the upper 5th percentile computed for stationary GARCH(1,1) process. Right subfigure: relationship between time series sample size and width of 95% confidence intervals for ES in the upper 5th percentile computed for stationary GARCH(1,1) process. Each plotted point is the averaged result over 10,000 replications.

Figure A.3: Coverage Probability and Confidence Intervals for GARCH(1,1) with i.i.d. Normal Innovations and Parameters $\lambda_1 = 0.1$ and $\lambda_2 = 0.6$



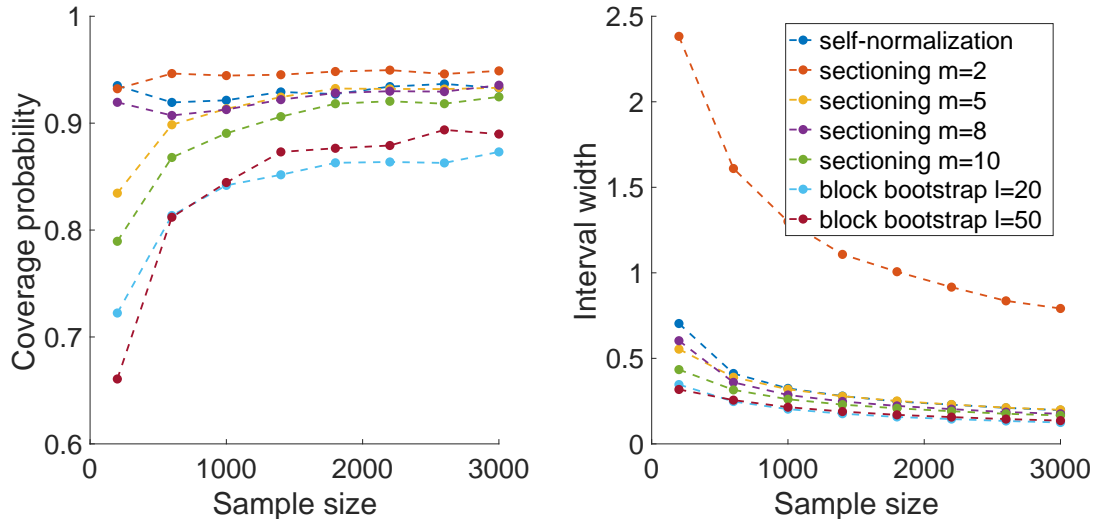
This figure shows the coverage probability and confidence interval width for different sample size. We use the GARCH(1,1) process with i.i.d. standard normal innovations, and set the model parameters as $\omega = 0.01$, $\lambda_1 = 0.1$, and $\lambda_2 = 0.6$. Left subfigure: relationship between sample size and empirical coverage probability of 95% confidence intervals for ES in the upper 5th percentile computed for stationary GARCH(1,1) process. Right subfigure: relationship between time series sample size and width of 95% confidence intervals for ES in the upper 5th percentile computed for stationary GARCH(1,1) process. Each plotted point is the averaged result over 10,000 replications.

Figure A.4: Coverage Probability and Confidence Intervals for GARCH(1,1) with i.i.d. Normal Innovations and Parameters $\lambda_1 = 0.1$ and $\lambda_2 = 0.5$



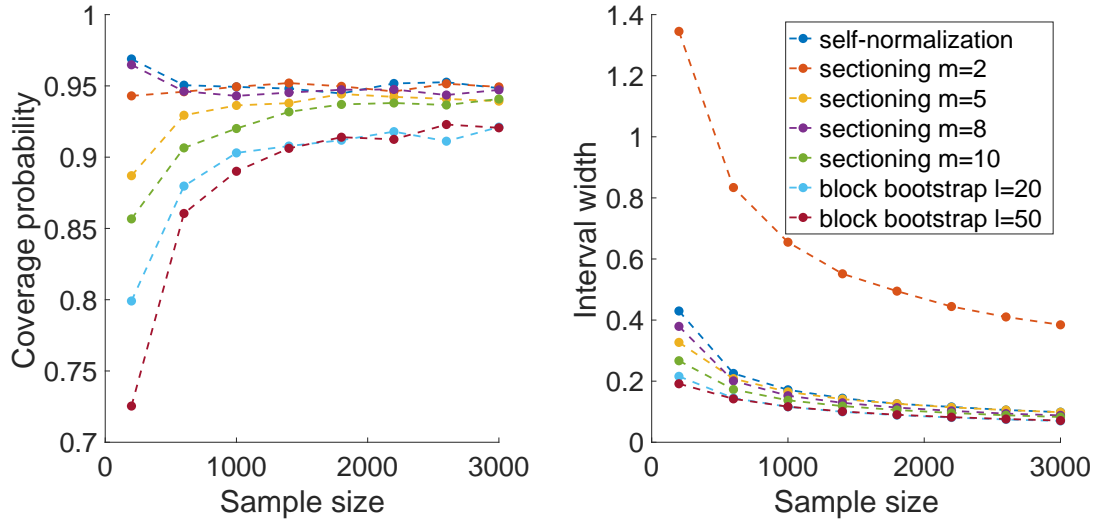
This figure shows the coverage probability and confidence interval width for different sample size. We use the GARCH(1,1) process with i.i.d. standard normal innovations, and set the model parameters as $\omega = 0.01$, $\lambda_1 = 0.1$, and $\lambda_2 = 0.5$. Left subfigure: relationship between sample size and empirical coverage probability of 95% confidence intervals for ES in the upper 5th percentile computed for stationary GARCH(1,1) process. Right subfigure: relationship between time series sample size and width of 95% confidence intervals for ES in the upper 5th percentile computed for stationary GARCH(1,1) process. Each plotted point is the averaged result over 10,000 replications.

Figure A.5: Coverage Probability and Confidence Intervals for GARCH(1,1) with i.i.d. $t(15)$ -Distributed Innovations and Parameters $\lambda_1 = 0.1$ and $\lambda_2 = 0.8$



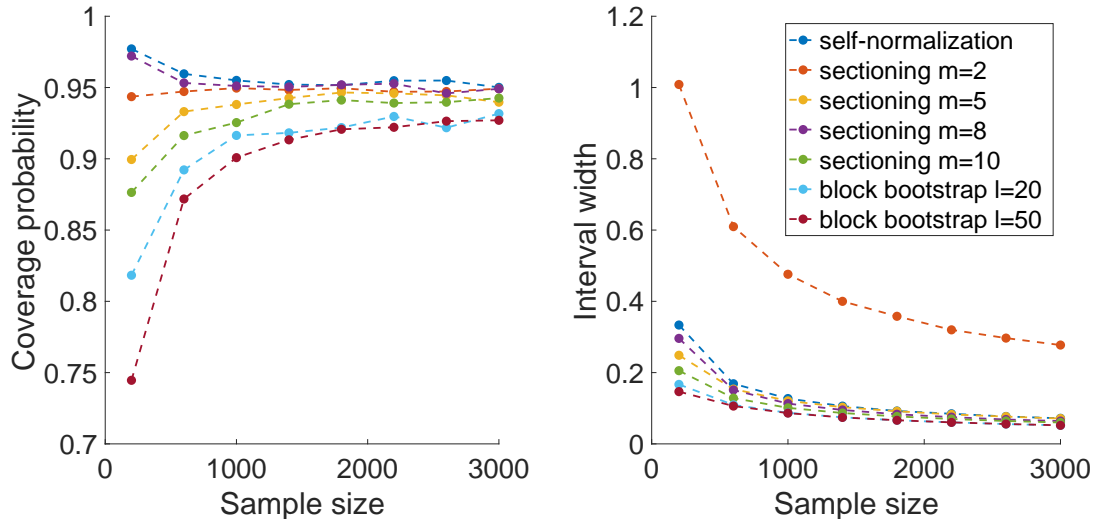
This figure shows the coverage probability and confidence interval width for different sample size. We use the GARCH(1,1) process with i.i.d. $t(15)$ -distributed innovations, and set the model parameters as $\omega = 0.01$, $\lambda_1 = 0.1$, and $\lambda_2 = 0.8$. Left subfigure: relationship between sample size and empirical coverage probability of 95% confidence intervals for ES in the upper 5th percentile computed for stationary GARCH(1,1) process. Right subfigure: relationship between time series sample size and width of 95% confidence intervals for ES in the upper 5th percentile computed for stationary GARCH(1,1) process. Each plotted point is the averaged result over 10,000 replications.

Figure A.6: Coverage Probability and Confidence Intervals for GARCH(1,1) with i.i.d. $t(15)$ -Distributed Innovations and Parameters $\lambda_1 = 0.1$ and $\lambda_2 = 0.7$



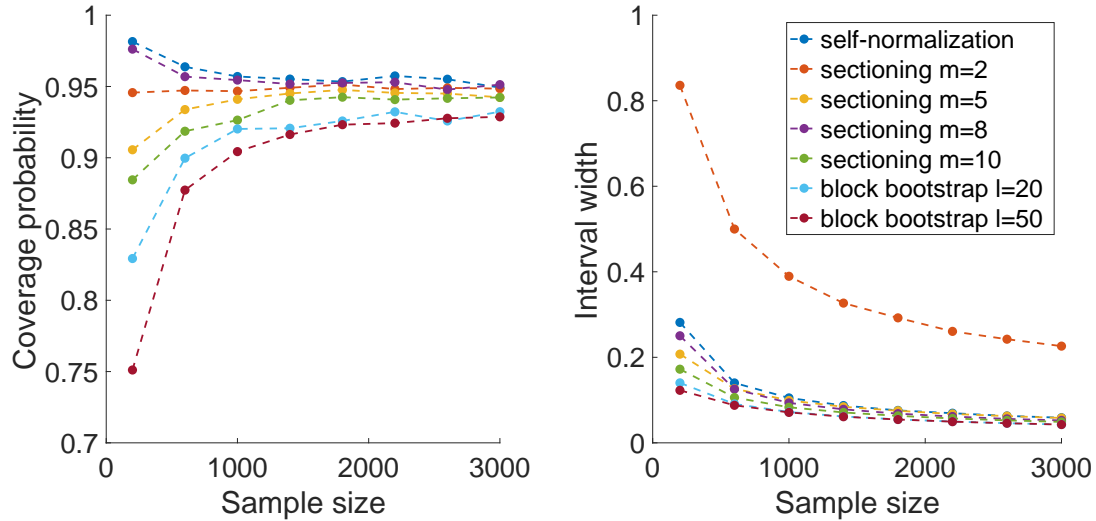
This figure shows the coverage probability and confidence interval width for different sample size. We use the GARCH(1,1) process with i.i.d. $t(15)$ -distributed innovations, and set the model parameters as $\omega = 0.01$, $\lambda_1 = 0.1$, and $\lambda_2 = 0.7$. Left subfigure: relationship between sample size and empirical coverage probability of 95% confidence intervals for ES in the upper 5th percentile computed for stationary GARCH(1,1) process. Right subfigure: relationship between time series sample size and width of 95% confidence intervals for ES in the upper 5th percentile computed for stationary GARCH(1,1) process. Each plotted point is the averaged result over 10,000 replications.

Figure A.7: Coverage Probability and Confidence Intervals for GARCH(1,1) with i.i.d. $t(15)$ -Distributed Innovations and Parameters $\lambda_1 = 0.1$ and $\lambda_2 = 0.6$



This figure shows the coverage probability and confidence interval width for different sample size. We use the GARCH(1,1) process with i.i.d. $t(15)$ -distributed innovations, and set the model parameters as $\omega = 0.01$, $\lambda_1 = 0.1$, and $\lambda_2 = 0.6$. Left subfigure: relationship between sample size and empirical coverage probability of 95% confidence intervals for ES in the upper 5th percentile computed for stationary GARCH(1,1) process. Right subfigure: relationship between time series sample size and width of 95% confidence intervals for ES in the upper 5th percentile computed for stationary GARCH(1,1) process. Each plotted point is the averaged result over 10,000 replications.

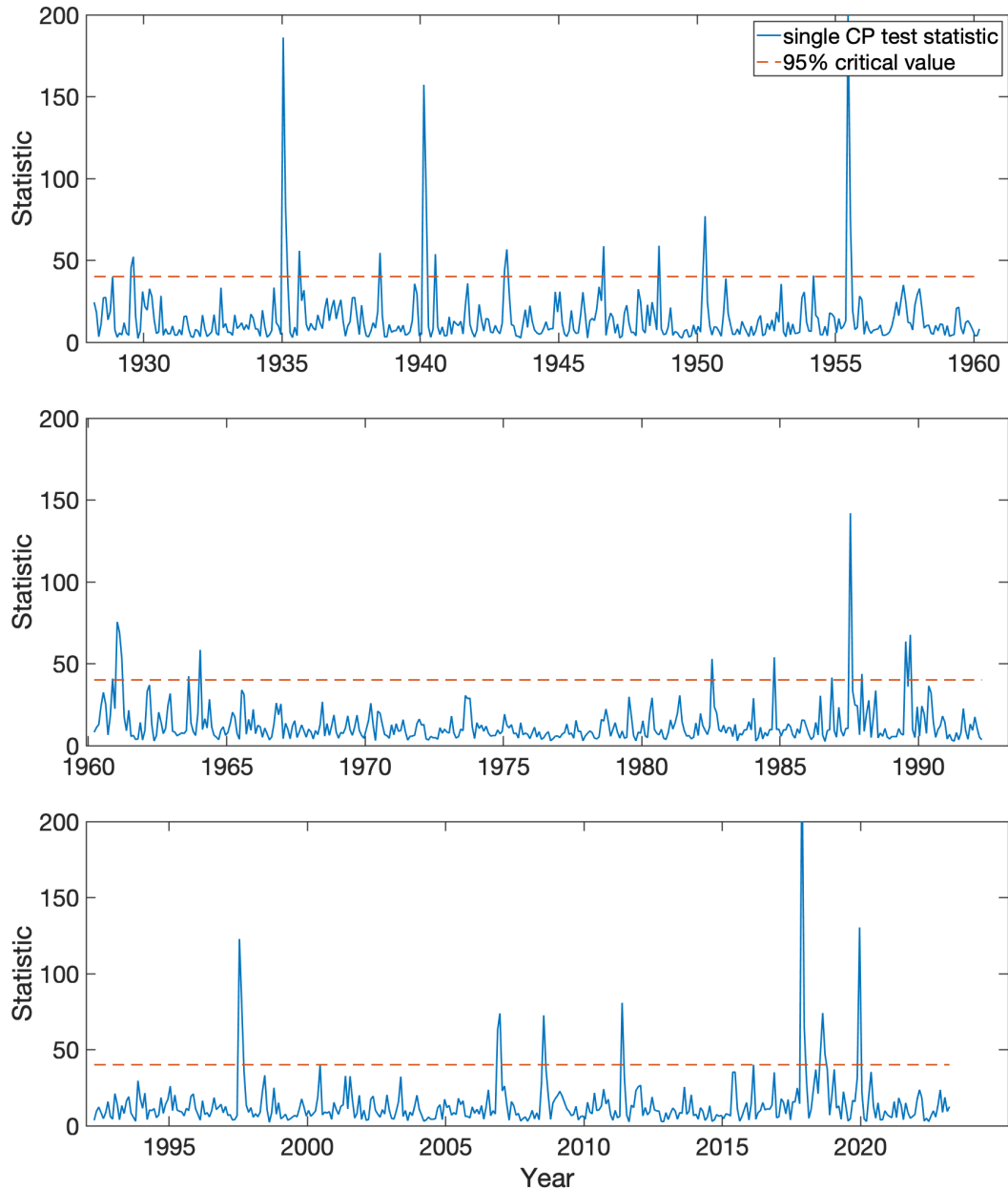
Figure A.8: Coverage Probability and Confidence Intervals for GARCH(1,1) with i.i.d. $t(15)$ -Distributed Innovations and Parameters $\lambda_1 = 0.1$ and $\lambda_2 = 0.5$



This figure shows the coverage probability and confidence interval width for different sample size. We use the GARCH(1,1) process with i.i.d. $t(15)$ -distributed innovations, and set the model parameters as $\omega = 0.01$, $\lambda_1 = 0.1$, and $\lambda_2 = 0.5$. Left subfigure: relationship between sample size and empirical coverage probability of 95% confidence intervals for ES in the upper 5th percentile computed for stationary GARCH(1,1) process. Right subfigure: relationship between time series sample size and width of 95% confidence intervals for ES in the upper 5th percentile computed for stationary GARCH(1,1) process. Each plotted point is the averaged result over 10,000 replications.

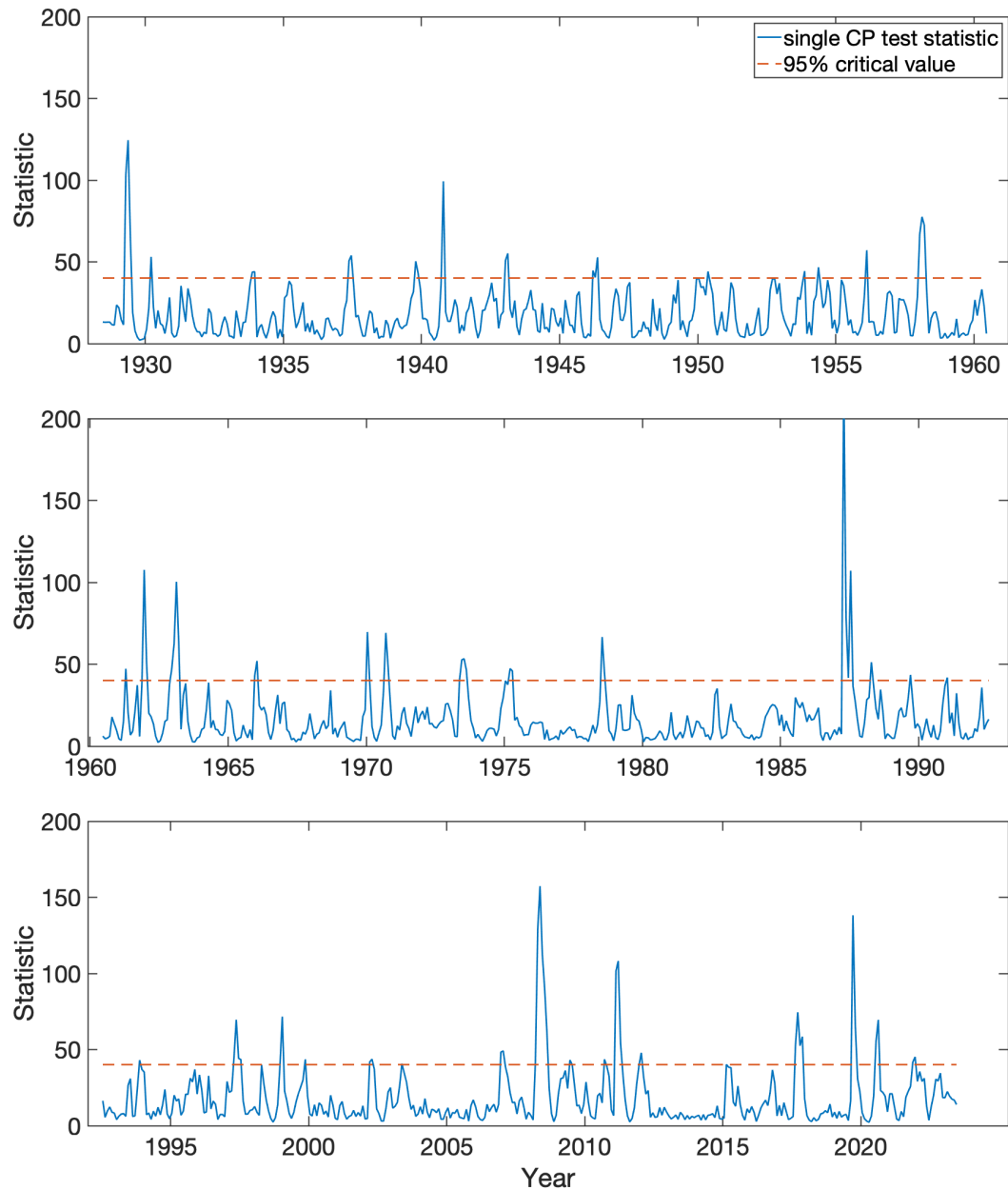
Appendix C: Empirical Results

Figure A.9: Single Change-Point Tests for S&P 500 Daily Returns with 6-Month Windows



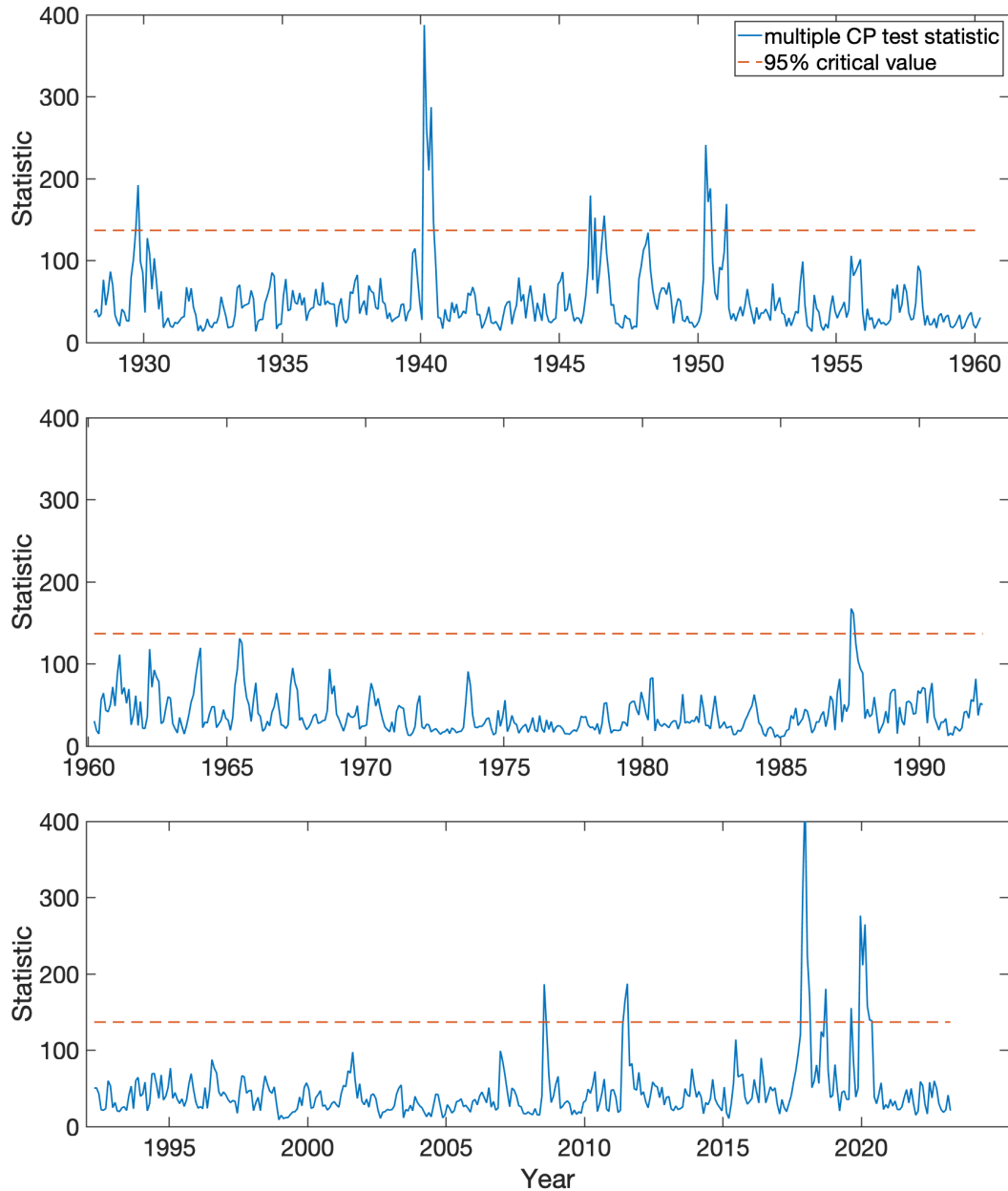
This figure shows the test statistics for single change-point tests for expected shortfall (ES) in the lower 5th percentile for S&P 500 log returns in different 6-month time windows.

Figure A.10: Single Change-Point Tests for S&P 500 Daily Returns with 12-Month Windows



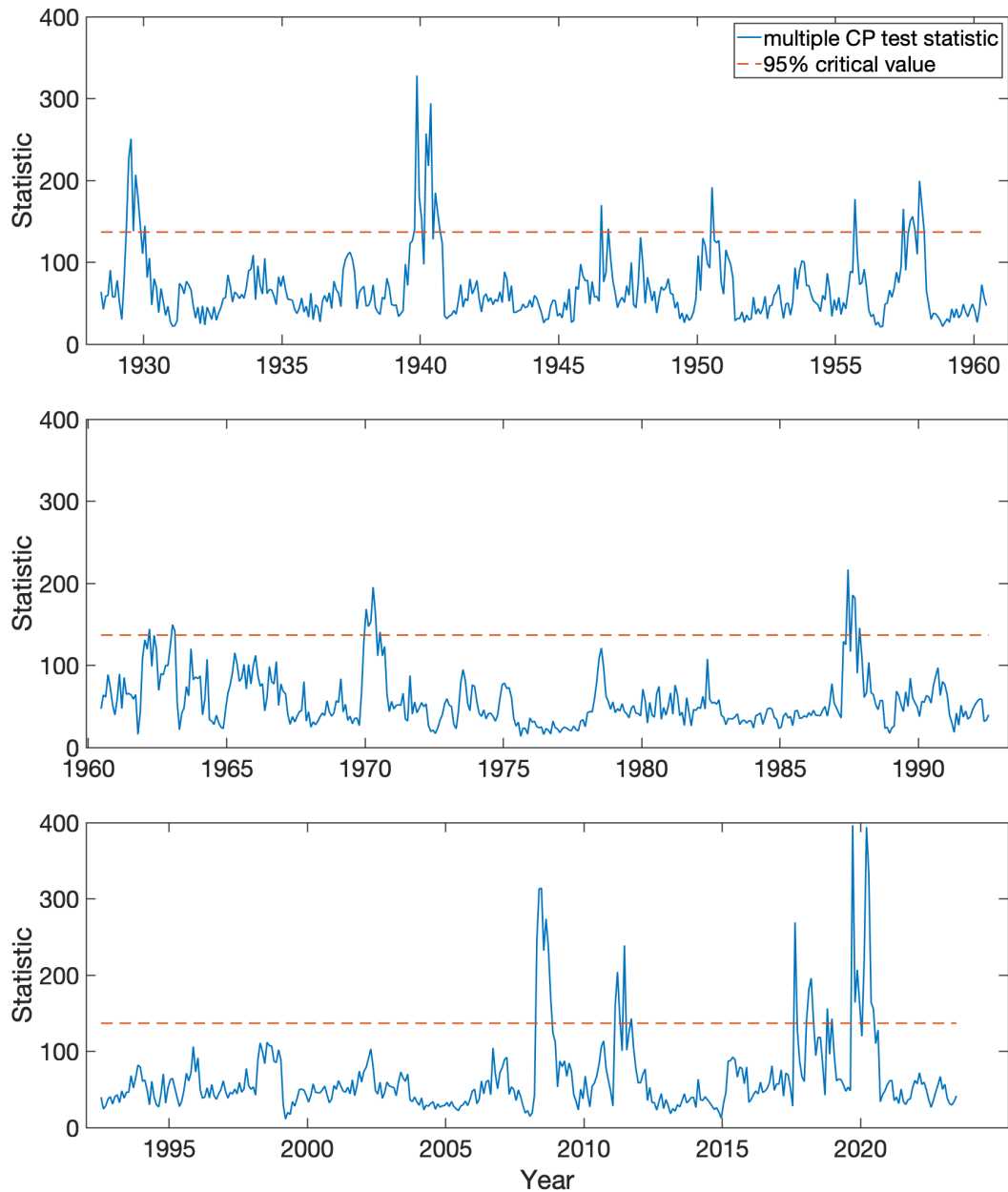
This figure shows the test statistics for single change-point tests for expected shortfall (ES) in the lower 5th percentile for S&P 500 log returns in different 12-month time windows.

Figure A.11: Multiple Change-Point Tests for S&P 500 Daily Returns with 6-Month Windows



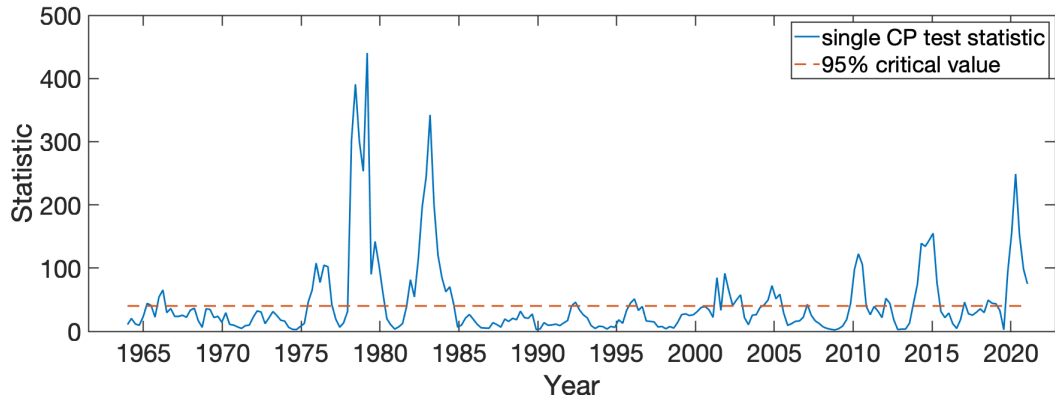
This figure shows the test statistics for multiple change-point tests for expected shortfall (ES) in the lower 5th percentile for S&P 500 log returns in different 6-month time windows.

Figure A.12: Multiple Change-Point Tests for S&P 500 Daily Returns with 12-Month Windows

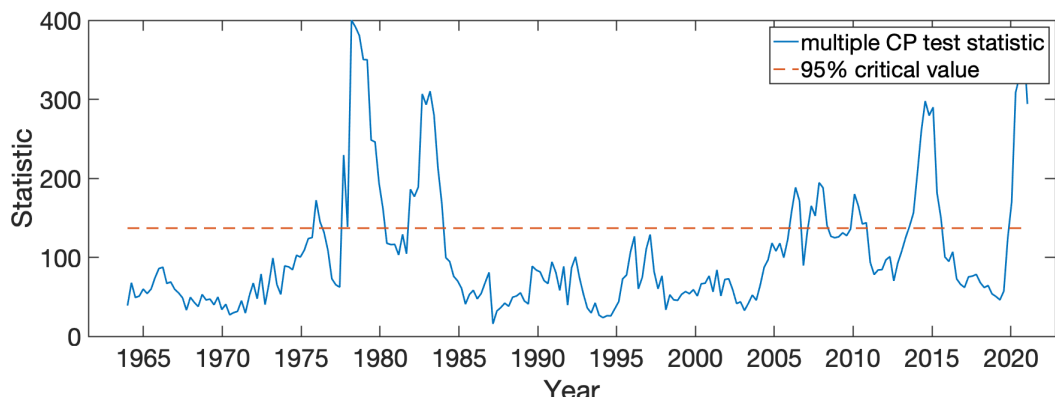


This figure shows the test statistics for multiple change-point tests for expected shortfall (ES) in the lower 5th percentile for S&P 500 log returns in different 12-month time windows.

Figure A.13: Change-Point Tests for U.S. 1-Year Bond Weekly Returns with 5-Year Windows



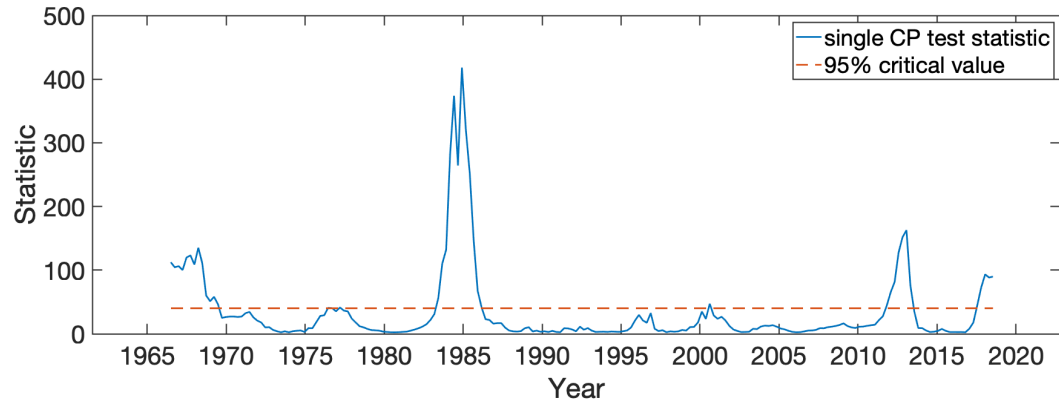
(a) Single change-point test statistics



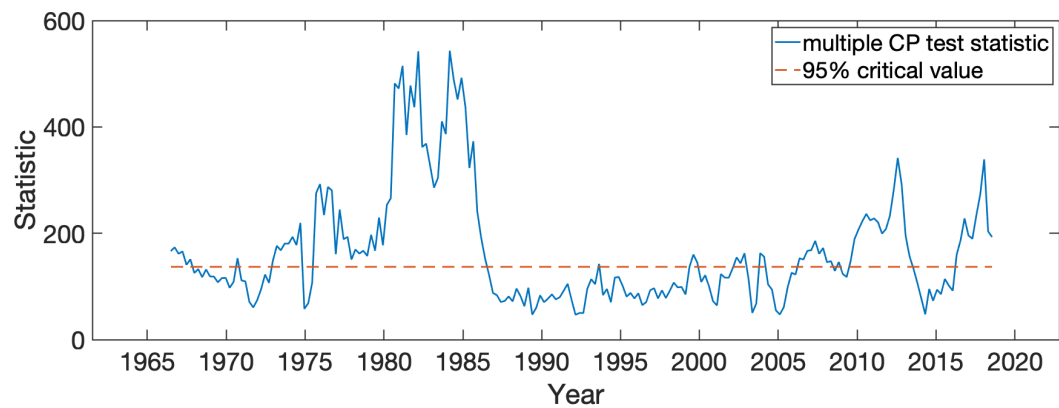
(b) Multiple change-point test statistics

This figure shows the test statistics for single and multiple change-point tests for expected shortfall (ES) in the lower 10th percentile for U.S. 1-year zero-coupon bond log returns in different 5-year time windows.

Figure A.14: Change-Point Tests for U.S. 1-Year Bond Weekly Returns with 10-Year Windows



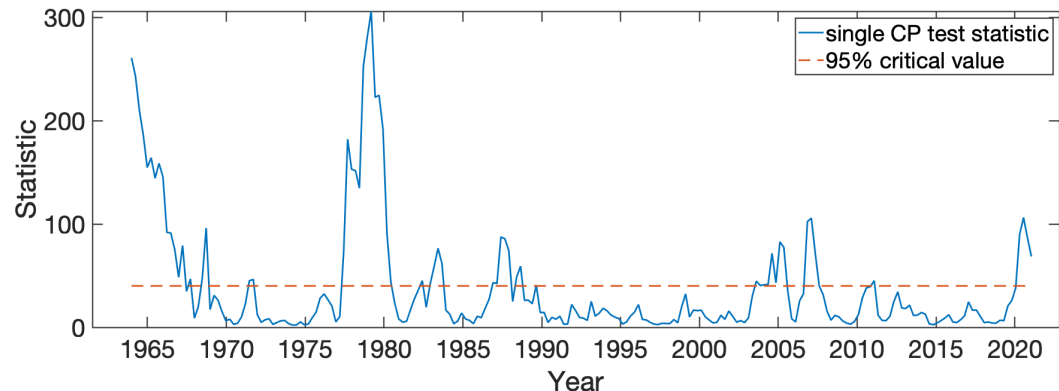
(a) Single change-point test statistics



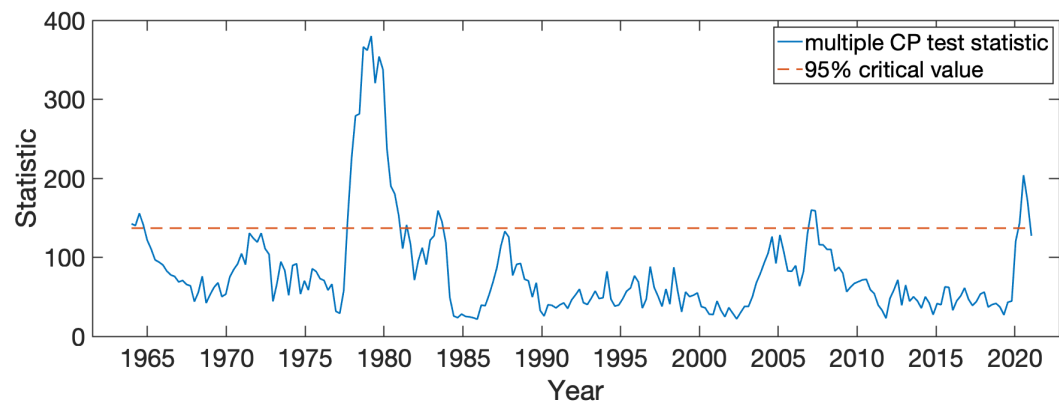
(b) Multiple change-point test statistics

This figure shows the test statistics for single and multiple change-point tests for expected shortfall (ES) in the lower 10th percentile for U.S. 1-year zero-coupon bond log returns in different 10-year time windows.

Figure A.15: Change-Point Tests for U.S. 10-Year Bond Weekly Returns with 5-Year Windows



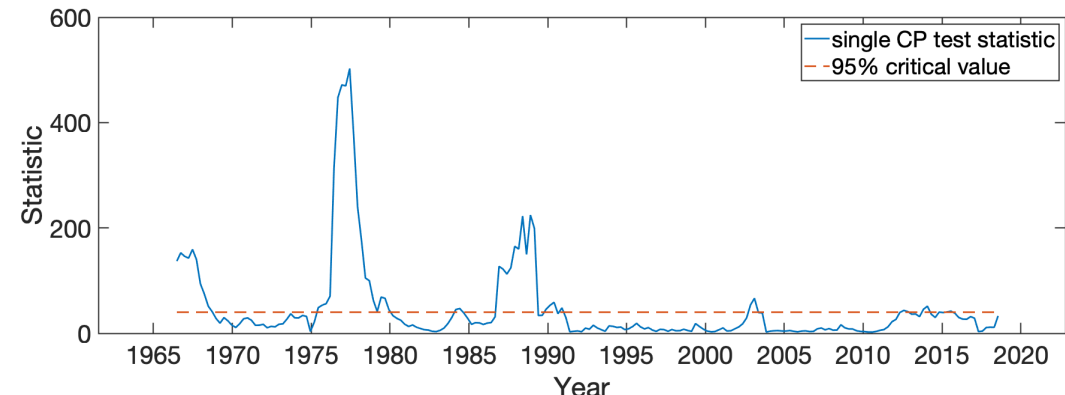
(a) Single change-point test statistics



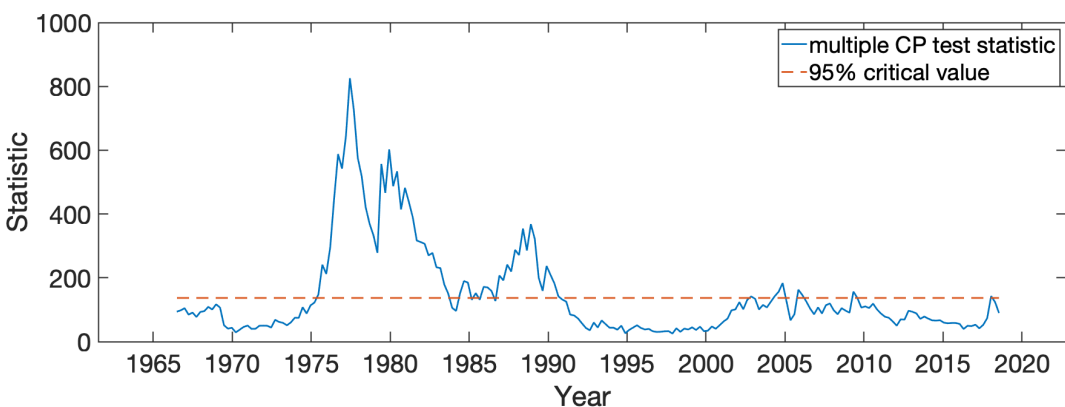
(b) Multiple change-point test statistics

This figure shows the test statistics for single and multiple change-point tests for expected shortfall (ES) in the lower 10th percentile for U.S. 10-year zero-coupon bond log returns in different 5-year time windows.

Figure A.16: Change-Point Tests for U.S. 10-Year Bond Weekly Returns with 10-Year Windows



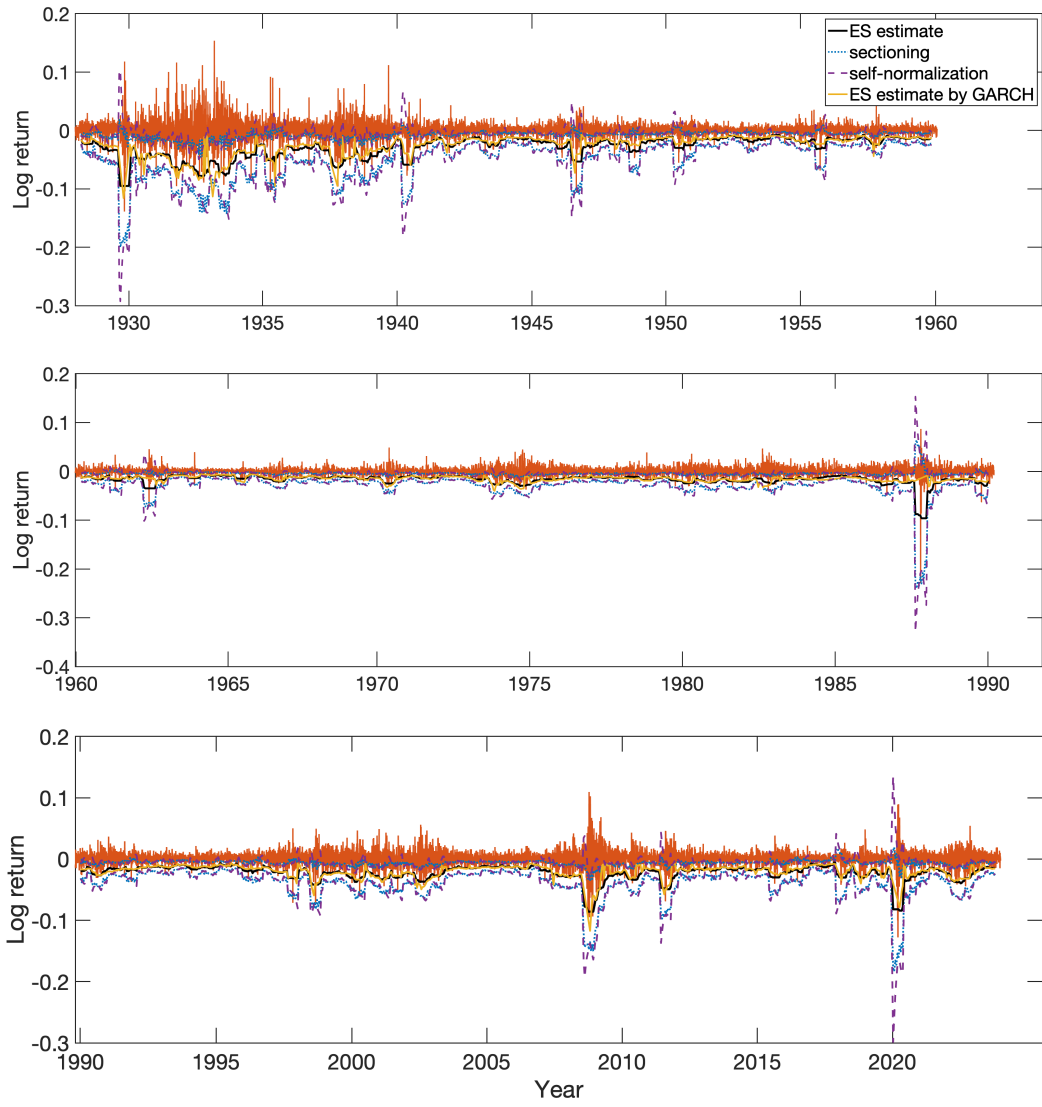
(a) Single change-point test statistics



(b) Multiple change-point test statistics

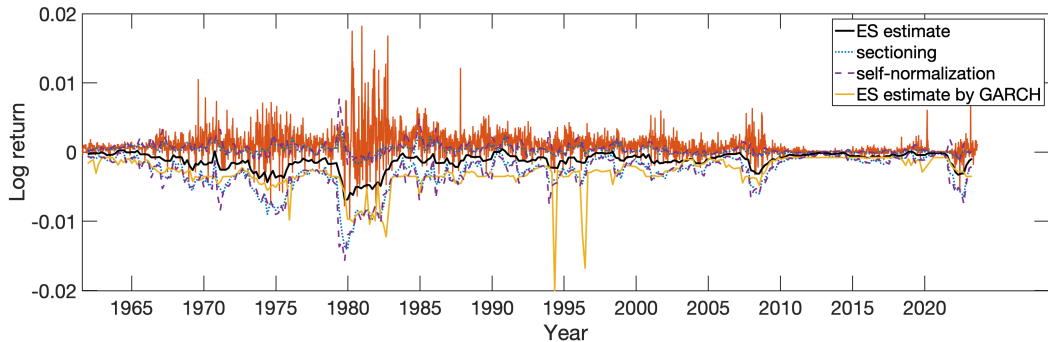
This figure shows the test statistics for single and multiple change-point tests for expected shortfall (ES) in the lower 10th percentile for U.S. 10-year zero-coupon bond log returns in different 10-year time windows.

Figure A.17: Expected Shortfall of Market Returns over Time

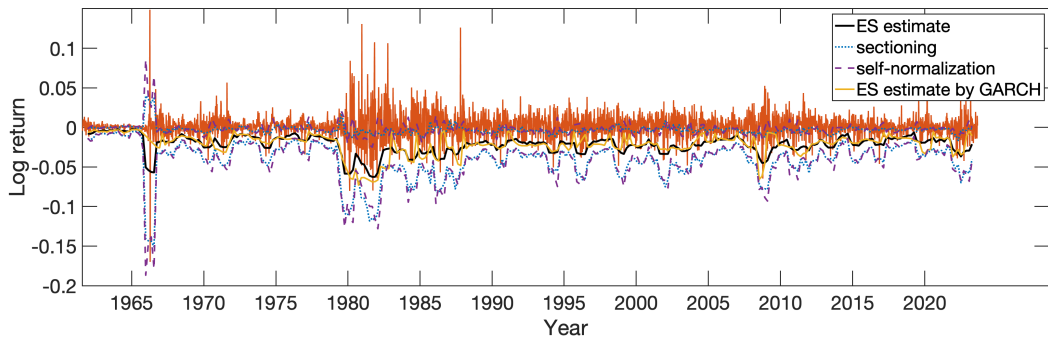


This figure shows the daily log returns and expected shortfall with confidence intervals for the S&P 500 index that approximates a market return time-series. We plot the ES estimate and 95% confidence bands for the lower 5th percentile. ES is computed using a rolling window of 100 days with 10 day shifts.

Figure A.18: Expected Shortfall of Bond Returns over Time



(a) U.S. 1-year zero-coupon bond



(b) U.S. 10-year zero-coupon bond

This figure shows the weekly log returns and expected shortfall with confidence intervals for long- and short-maturity zero-coupon bonds. We plot the ES estimate and 95% confidence bands for the lower 10th percentile of log returns. ES is computed using a rolling window of 40 weeks with 10 week shifts.

Table A.1: B-Y Multiple Testing Adjustments for Change-Point Tests for Bond Returns

time window	single CP test		multiple CP test	
	statistic	p-value	statistic	p-value
US 1-year bond weekly log returns				
03/21/1976 - 03/08/1981	300.3	<0.001	380.7	<0.001
09/16/1979 - 08/27/1989	264.3	<0.001	451.5	<0.001
09/14/1980 - 09/01/1985	342.3	<0.001	310.3	0.001
10/29/2017 - 10/16/2022	248.9	<0.001	308.7	0.001
09/27/1970 - 09/07/1980	18.3	0.210	275.6	0.001
09/21/1975 - 09/01/1985	2.3	0.991	481.7	<0.001
03/19/1978 - 02/28/1988	30.9	0.090	285.8	0.001
09/14/1980 - 08/26/1990	146.2	0.001	373.0	<0.001
08/12/2007 - 07/23/2017	127.6	0.001	341.7	<0.001
11/04/2012 - 10/16/2022	72.7	0.011	273.3	0.001
04/29/2018 - 04/16/2023	98.9	0.003	375.6	<0.001
US 10-year bond weekly log returns				
06/25/1972 - 06/06/1982	502.6	<0.001	825.6	<0.001
06/20/1976 - 06/07/1981	281.0	<0.001	361.9	<0.001
03/11/1984 - 02/20/1994	199.2	0.001	321.8	<0.001
07/09/1961 - 06/26/1966	260.9	<0.001	142.4	0.043
03/28/1971 - 03/08/1981	70.5	0.012	295.2	0.001
06/24/1973 - 06/05/1983	104.9	0.002	422.0	<0.001
06/19/1977 - 05/31/1987	6.2	0.581	270.1	0.001
06/12/1983 - 05/23/1993	222.5	0.001	354.1	<0.001

In this table, we consider B-Y multiple hypothesis testing adjustments to single and multiple change-point tests for expected shortfall (ES) in the lower 10th percentile for U.S. 1-year and 10-year zero-coupon bond weekly log returns over the rolling windows in Figures A.13-A.16. Separately for each sub-figure of Figures A.13-A.16, we apply the B-Y procedure with FDR control level of 0.05 to all windows (each corresponding to a separate change-point test) within that sub-figure. (Recall that the setup for these windows was discussed in Section 5.2. Also, see below for the details of the B-Y procedure.) The top blocks report the windows that the B-Y procedure finds significant for both the single and multiple change-point tests. The middle blocks report the windows that the B-Y procedure finds significant for the single change-point test, but not for the multiple change-point test. The lower blocks report the windows that the B-Y procedure finds significant for the multiple change-point test, but not for the single change-point test. For each window, we also report the raw change-point test statistics and corresponding p-values.

Benjamini-Yekutieli (B-Y) Procedure (Benjamini and Yekutieli, 2001)

The B-Y procedure for FDR control at level $\alpha \in (0, 1)$ consists of the following. We are given a list of p-values p_1, \dots, p_m and corresponding null hypotheses h_1, \dots, h_m . We first order the p-values in ascending order: $p_{(1)}, \dots, p_{(m)}$, with corresponding null hypotheses ordered accordingly: $h_{(1)}, \dots, h_{(m)}$. Next, we find the largest k such that $p_{(k)} \leq (k \cdot \alpha)/(m \cdot c_m)$, where $c_m = \sum_{j=1}^m j^{-1}$. Then, at FDR level α , we reject the null hypotheses: $h_{(1)}, \dots, h_{(k)}$ (declaring them to be discoveries/significant).